NATIONAL ADVISORY COMMITTEE FOR AERONAUTICS

REPORT No. 725 c. 3

EFFECT OF BODY NOSE SHAPE ON THE PROPULSIVE EFFICIENCY OF A PROPELLER

By GEORGE W. STICKLE, JOHN L. CRIGLER, and IRVEN NAIMEN

1941

AERONAUTIC SYMBOLS

1. FUNDAMENTAL AND DERIVED UNITS

	Symbol	Metric		English	
		Unit	Abbreviation	Unit	Abbreviation
Length	l	meter	m	foot (or mile)	ft (or mi)
Time	t	second	s	second (or hour)	sec (or hr)
Force	F	weight of 1 kilogram	kg	weight of 1 pound	lb
Power	P	horsepower (metric)		horsepower	hp
Speed	V	kilometers per hour	kph	miles per hour	mph
		meters per second	mps	feet per second	fps

2. GENERAL SYMBOLS

W Weight$=mg$

g Standard acceleration of gravity$=9.80665$ m/s^2 or 32.1740 ft/sec^2

m Mass$=\frac{W}{g}$

I Moment of inertia$=mk^2$. (Indicate axis of radius of gyration k by proper subscript.)

μ Coefficient of viscosity

ν Kinematic viscosity

ρ Density (mass per unit volume)

Standard density of dry air, 0.12497 kg-m^{-4}-s^2 at 15° C and 760 mm; or 0.002378 lb-ft^{-4} sec^2

Specific weight of "standard" air, 1.2255 kg/m^3 or 0.07651 lb/cu ft

3. AERODYNAMIC SYMBOLS

S Area

S_w Area of wing

G Gap

b Span

c Chord

A Aspect ratio, $\frac{b^2}{S}$

V True air speed

q Dynamic pressure, $\frac{1}{2}\rho V^2$

L Lift, absolute coefficient $C_L=\frac{L}{qS}$

D Drag, absolute coefficient $C_D=\frac{D}{qS}$

D_0 Profile drag, absolute coefficient $C_{D_0}=\frac{D_0}{qS}$

D_i Induced drag, absolute coefficient $C_{D_i}=\frac{D_i}{qS}$

D_p Parasite drag, absolute coefficient $C_{D_p}=\frac{D_p}{qS}$

C Cross-wind force, absolute coefficient $C_C=\frac{C}{qS}$

i_w Angle of setting of wings (relative to thrust line)

i_t Angle of stabilizer setting (relative to thrust line)

Q Resultant moment

Ω Resultant angular velocity

R Reynolds number, $\rho\frac{Vl}{\mu}$ where l is a linear dimension (e.g., for an airfoil of 1.0 ft chord, 100 mph, standard pressure at 15° C, the corresponding Reynolds number is 935,400; or for an airfoil of 1.0 m chord, 100 mps, the corresponding Reynolds number is 6,865,000)

α Angle of attack

ϵ Angle of downwash

α_0 Angle of attack, infinite aspect ratio

α_i Angle of attack, induced

α_a Angle of attack, absolute (measured from zero-lift position)

γ Flight-path angle

REPORT No. 725

EFFECT OF BODY NOSE SHAPE ON THE PROPULSIVE EFFICIENCY OF A PROPELLER

By GEORGE W. STICKLE, JOHN L. CRIGLER, and IRVEN NAIMEN

Langley Memorial Aeronautical Laboratory

NATIONAL ADVISORY COMMITTEE FOR AERONAUTICS

HEADQUARTERS, NAVY BUILDING, WASHINGTON, D. C.

Created by act of Congress approved March 3, 1915, for the supervision and direction of the scientific study of the problems of flight (U. S. Code, Title 50, Sec. 151). Its membership was increased to 15 by act approved March 2, 1929. The members are appointed by the President, and serve as such without compensation.

TECHNICAL COMMITTEES

AERODYNAMICS
POWER PLANTS FOR AIRCRAFT
AIRCRAFT MATERIALS

AIRCRAFT STRUCTURES
AIRCRAFT ACCIDENTS
INVENTIONS AND DESIGNS

Coordination of Research Needs of Military and Civil Aviation

Preparation of Research Programs

Allocation of Problems

Prevention of Duplication

Consideration of Inventions

LANGLEY MEMORIAL AERONAUTICAL LABORATORY

LANGLEY FIELD, VA.

AMES AERONAUTICAL LABORATORY

MOFFETT FIELD, CALIF.

Conduct, under unified control, for all agencies, of scientific research on the fundamental problems of flight.

OFFICE OF AERONAUTICAL INTELLIGENCE

WASHINGTON, D. C.

Collection, classification, compilation, and dissemination of scientific and technical information on aeronautics

REPORT No. 725

EFFECT OF BODY NOSE SHAPE ON THE PROPULSIVE EFFICIENCY OF A PROPELLER

By George W. Stickle, John L. Crigler, and Irven Naiman

SUMMARY

Three adjustable propellers of 10-foot diameter were operated in front of four body nose shapes, varying from a streamline nose that continued through the propeller plane in the form of a large spinner to a conventional open-nose radial-engine cowling. One propeller had airfoil sections close to the hub, the second had conventional round blade shanks, and the third differed from the second only in pitch distribution. The blade-angle settings ranged from 20° to 55° at the 0.75 radius.

The effect of the body nose shape on propulsive efficiency may be divided into two parts: (1) the change in the body drag due to the propeller slipstream and (2) the change in propeller load distribution due to the change in velocity caused by the body. For the nose shape tested in this report, the first effect is shown to be very small; therefore, the chief emphasis of the report is confined to the second effect.

The results showed that, in the design of the pitch distribution, proper consideration should be given to the velocity field produced by the presence of the body adjacent to the propeller.

The presence of a body behind the propeller produces its greatest effect on the inner sections of the propeller blades. When the inner sections are of conventional round-shank design, the important effect is the change in the drag of these sections due to the reduced velocity in front of the body. For inner sections of an airfoil design, the main effect is the change of the load distribution of the propeller due to increasing the angle of attack by reduction of the forward velocity. The gain in efficiency realized by covering the propeller hub with a spinner is a function of the local velocity to which the hub is exposed; the possible gain increases as the power loading decreases.

INTRODUCTION

The tests reported in reference 1 showed that the characteristics of a propeller are dependent on the body behind the propeller. The difference in the velocity distribution in front of two open-nose NACA cowlings caused a change of 5 percent in the propulsive efficiency.

A propeller that had a constant pitch distribution when set 30° at the 0.75 radius was shown by the tests of reference 1 to give higher propulsive efficiencies than a similar propeller with a constant pitch distribution when set 12° at the 0.75 radius. Tests reported in reference 2 showed a reverse effect of pitch distribution for propellers of a different plan form; the propeller that had a constant pitch distribution when set 35° at the 0.75 radius gave slightly lower efficiencies over the entire high-speed flight range than the one set 15°. The results shown in reference 1 indicated the possibility that these apparently contradictory results of the effect of pitch distribution might be explained by the effect of the body shape in changing the local angle of attack of the propeller sections.

This report presents results of three full-scale propellers tested in front of several nose shapes. The body shapes ranged from a streamline nose extending through the propeller disk with a large spinner to the normal type of blunt-shape, open-nose cowling. The results indicate how the body shape affects the local pitch distribution and the charts show the effects of this change on the propulsive efficiency.

SYMBOLS

h	thickness of blade sections of propeller
b	width of blade sections of propeller
r	station radius of propeller
R	tip radius of propeller
x	fraction of tip radius (r/R)
D	diameter of propeller
V	velocity of free air stream
n	revolutions per unit time of propeller
V/nD	advance-diameter ratio of propeller
p	geometric pitch of propeller
β	propeller blade-angle setting at $0.75R$
θ	propeller blade angle
u_0	velocity in plane of propeller, propeller removed
ρ	mass density of air
q	dynamic pressure of air stream ($\frac{1}{2}\rho V^2$)
P	power input to propeller
C_P	power coefficient ($P/\rho n^3 D^3$)
R	net force on thrust balance of propeller-nacelle unit
D	drag of nacelle for corresponding airspeed measured with propeller removed
ΔD	change in nacelle drag due to spinner
C_D	drag coefficient (D/qF)
ΔC_D	change in nacelle drag coefficient due to spinner ($\Delta D/qF$)
ΔD_P	change in nacelle drag due to propeller slipstream
ΔC_{D_P}	change in nacelle drag coefficient due to propeller slipstream (D_P/qF)

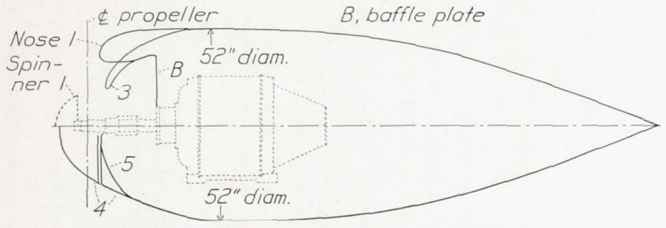

FIGURE 1.—Line drawing of the test arrangements.

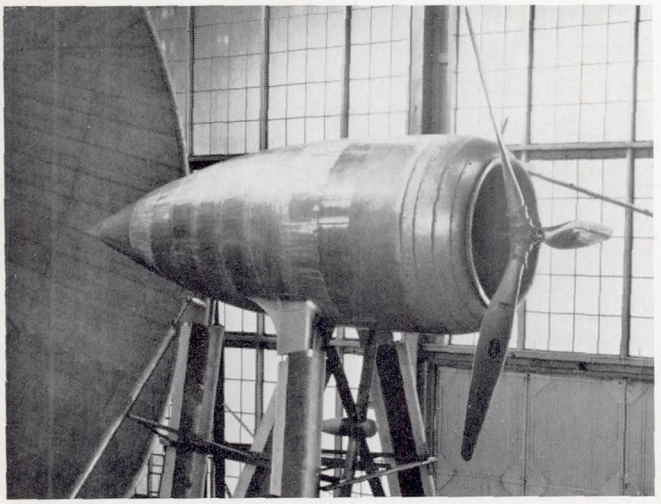

FIGURE 2.—Nose 1. (Slot shown here was closed for tests in this report.)

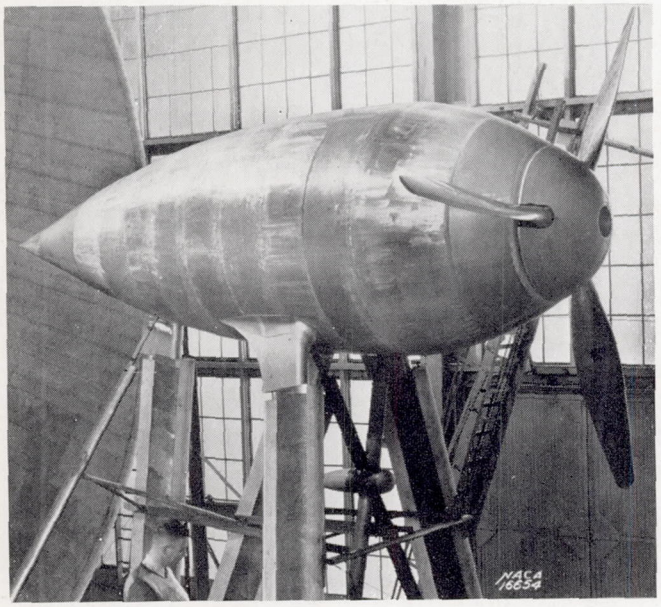

FIGURE 3.—Nose 4.

T propeller thrust (tension in crankshaft)
T_e effective thrust $(T-\Delta D_p)$
C_T effective thrust coefficient $(T_e/\rho n^2 D^4)$
T_c effective thrust disk-loading coefficient (T_e/qS)
F' projected frontal area of nacelle
S disk area of propeller
P_c power disk-loading coefficient (P/qSV)
$1/\sqrt[3]{P_c}=V\sqrt[3]{\rho S/2P}$
η_P propulsive efficiency (TV/P)
η propulsive efficiency $\left(\frac{(T-\Delta D_P)V}{P}\right)$
η' propulsive efficiency, the spinner being considered a part of the body
η_n net efficiency (RV/P)
C_s speed-power coefficient $(\sqrt[5]{\rho V^5/Pn^2})$
α_{a_0} angle of attack for zero lift for blade section

APPARATUS AND TESTS

Figure 1 presents a line drawing of the nacelle: the four noses, the afterbody shape, and spinner 1, which was used in conjunction with noses 3 and 5. Nose 4 extended through the propeller disk in the form of a large spinner that was considered to be a part of the body. Spinner 1 was considered to be a part of the propeller instead of a part of the body; the change in

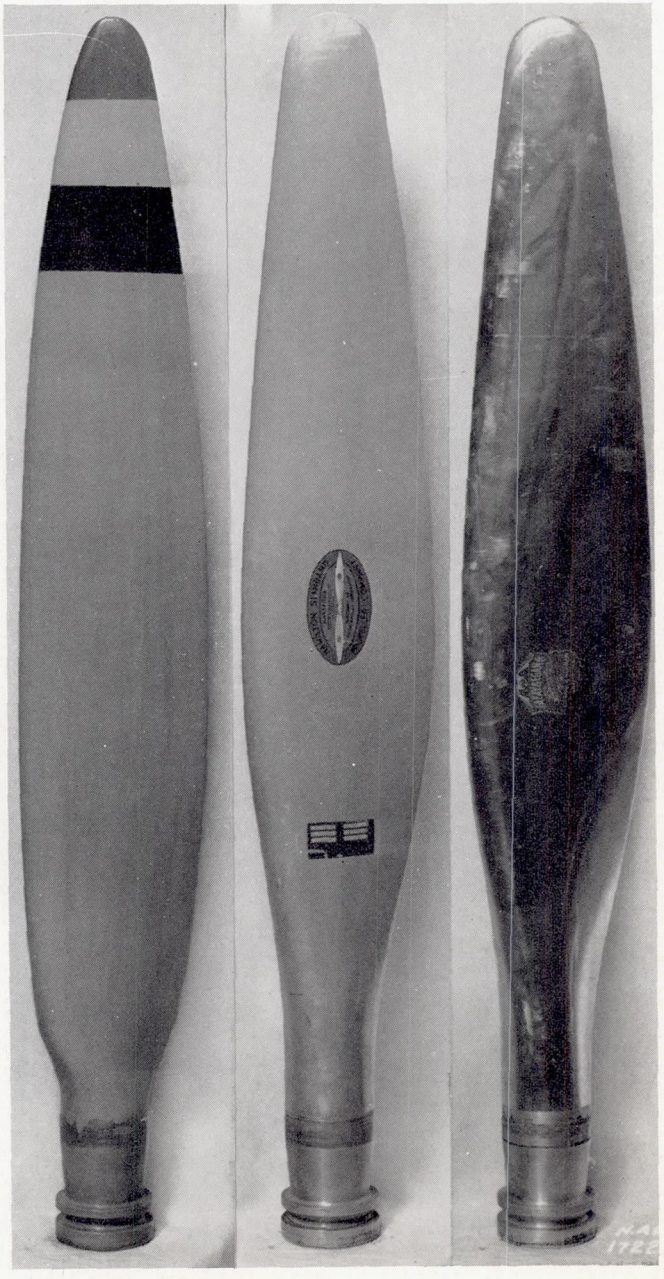

FIGURE 4.—One blade of each of the three propellers used.

body drag caused by spinner 1 was therefore disregarded in computing the propulsive efficiency.

The tests were conducted in the NACA 20-foot wind tunnel described in reference 3. Figures 2 and 3 show the installations of noses 1 and 4 in the tunnel. A 150-horsepower variable-speed electric motor enclosed in the nacelle furnished power to the propeller.

Three adjustable propellers of Clark Y section were tested. Each propeller was 10 feet in diameter and had three blades. One blade of each propeller is shown in figure 4. Propeller F is Bureau of Aeronautics design drawing No. 4893. Propeller C is Bureau of Aeronautics drawing No. 5868–9. Propeller C_x is a modification in pitch distribution of propeller C and, in reference 2, is designated 5868–X_2. The blade-form curves are given in figure 5.

The geometric pitch p of a propeller section is the advance per revolution that would occur if the section were a straight line set at an angle θ to the plane of rotation and moving through a medium without slip; that is, without thrust and consequently without inflow, or

$$p=2\pi r \tan\theta=V/n$$

$$p/D=\pi x \tan\theta=V/nD$$

Thus, the given pitch distribution defines for each section a value of V/nD for which the chord line moves in the direction of the resultant of the axial and the circumferential velocities (interference velocities are neglected). In practice, the axial velocity relative to the section is not the velocity of advance V but a velocity u_0 caused by the blocking effect of the body. The condition to be satisfied is then:

$$\theta=\arctan\frac{u_0}{\pi x nD}$$

or

$$\pi x \tan\theta=\frac{u_0}{nD}$$

When this equation is multiplied by V/u_0, there results

$$\frac{p}{D}\frac{V}{u_0}=\pi x\frac{V}{u_0}\tan\theta=\frac{V}{nD}$$

This equation gives the value of V/nD for which the chord line of the section moves in the direction of the resultant velocity.

The velocity distribution in front of nose 1 is given in figure 6. The geometric pitch and the geometric pitch as modified by the local velocity in front of nose 1 are given in figure 7.

Inasmuch as the airfoil section used for most propellers is of a flat-bottom type (Clark Y, R. A. F. 6, etc.), when the chord line is set in the direction of motion, the section is from 3° to 7° above zero lift, depending upon the thickness. As will be shown later, at peak efficiency the propeller sections are usually working at an apparent angle of attack from 3° to 7° above zero lift. It is thus seen that, to a first approximation, the modified pitch distribution indicates how satisfactory the design pitch is at any particular value of V/nD.

Propellers F and C have approximately constant pitch when set 15° at $0.75R$; propeller C_x has been twisted to have approximately constant pitch over the outer half when set 35° at $0.75R$. Propellers C and C_x have round blade shanks near the hub; propeller F has airfoil sections extending nearer to the hub.

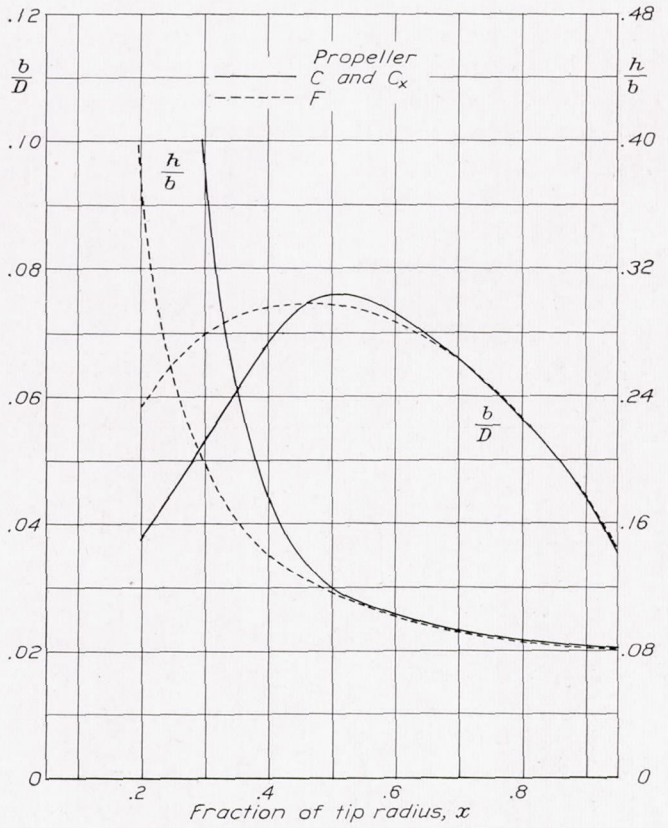

FIGURE 5.—Blade-form curves for propellers F, C, and C_x.

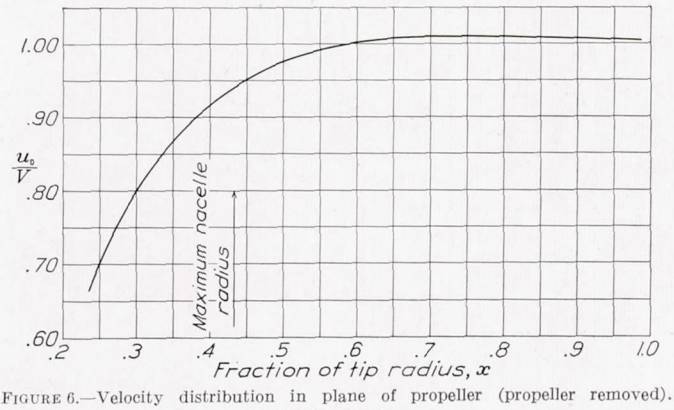

FIGURE 6.—Velocity distribution in plane of propeller (propeller removed). V, 93 miles per hour.

The tests covered a range of blade-angle settings from 20° to 55° at $0.75R$. Tunnel air speeds up to 110 miles per hour were used. All tests were made with zero air flow through the nacelle to eliminate the effect of the cowling pumping efficiency on the propeller results. The supports were shielded from the air stream as shown in figures 2 and 3. No corrections have been made for tare drag or horizontal buoyancy.

RESULTS

The original test points are given in figures 8 to 18, where the usual thrust coefficient C_T, power coefficient C_P, and propulsive efficiency η are plotted against V/nD. Each figure gives the complete range of blade-angle settings for one propeller tested in conjunction with one nose. Figure 19 shows the propulsive-efficiency envelopes against V/nD for nose 1 with propellers F and C. Figure 20 shows similar results for nose 3 and spinner 1 with all three propellers; figure 21 shows results for nose 4 with propellers C and C_X; and figure 22, for nose 5 and spinner 1 with all three propellers.

In figures 23 to 33, η has been plotted against $1/\sqrt[3]{P_c}$ for each propeller tested in conjunction with each nose. Figure 34 is a comparison of the propulsive-efficiency and the net-efficiency envelopes against $1/\sqrt[3]{P_c}$ for noses 1, 3, and 5 with all three propellers.

The drag results from tests without the propeller for all the noses are given in the following table:

Nose	D at $q=25.6$ lb/sq. ft (lb)	C_D	Remarks
1	30.5	0.0809	
3	30.3	.0802	
3	29.2	.0773	With spinner 1.
4	26.8	.0710	
5	27.5	.0728	
5	28.1	.0744	With spinner 1.

This table shows that the addition of spinner 1 decreased the total drag of nose 3 by 1.1 pounds but that the spinner increased the total drag of nose 5 by 0.6 pound. The change in the propulsive efficiency resulting from the addition of the spinner may be written as a function of the change in drag coefficient of the body, of P_c, and of the dimensions of the set-up:

$$\eta' = \eta + \frac{\Delta C_D}{P_c}\frac{F}{S}$$

where η' is the propulsive efficiency computed when the spinner is considered as part of the body. The high propulsive efficiency of nose 3 shown in figure 34 is the result of considering the spinner as part of the propeller. When the propulsive efficiency in figure 34 (a) is recomputed by considering the spinner as part of the body (i. e., by using the drag of the body with spinner), it is seen that the envelopes for noses 3 and 5 almost coincide (fig. 35).

The net-efficiency and the propulsive-efficiency envelopes are plotted against $1/\sqrt[3]{P_c}$ in figures 36 to 39.

Figures 40 to 43 are design charts included as an aid in determining the propeller diameter for conditions of high-speed flight. The use of this type of C_s curve for design characteristics is explained in the appendix of reference 1.

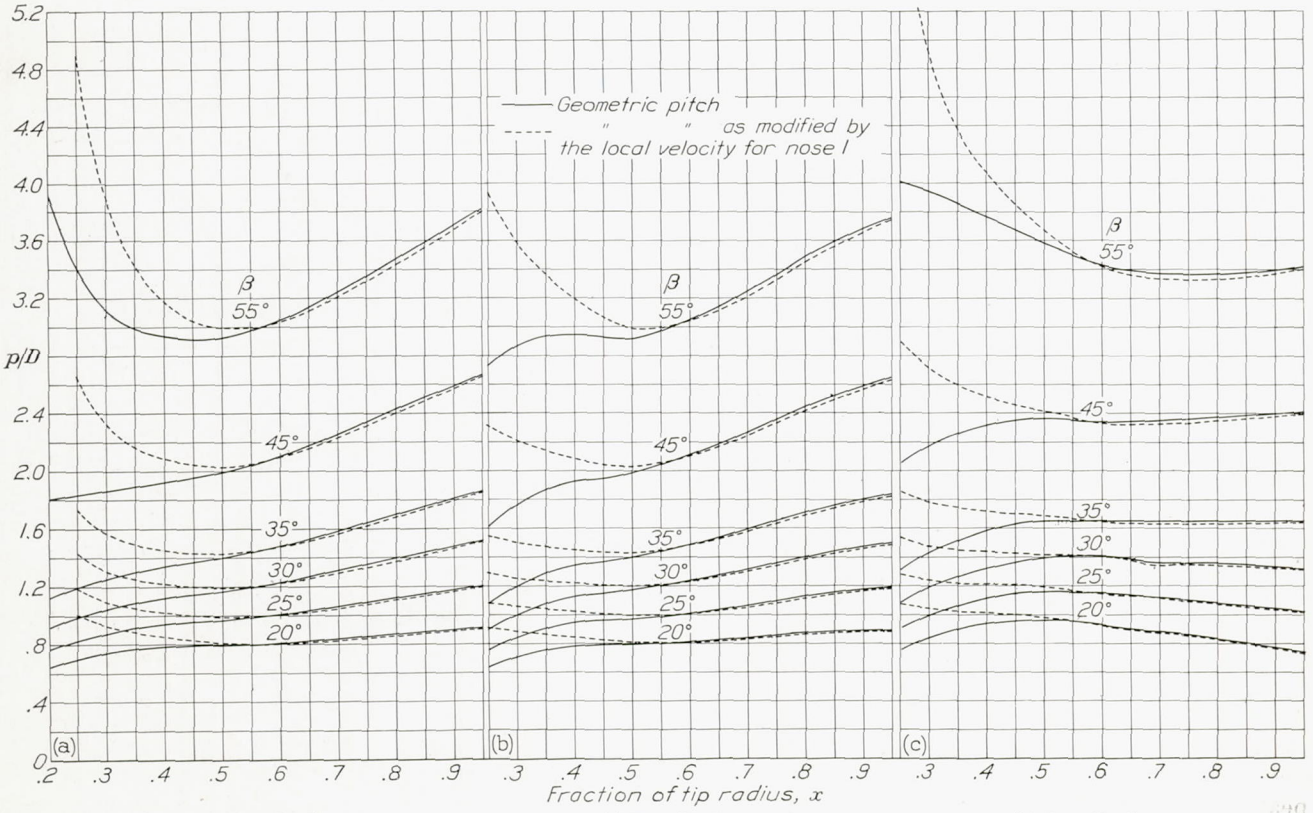

(a) Propeller F. (b) Propeller C. (c) Propeller C_x.

FIGURE 7.—Pitch distributions.

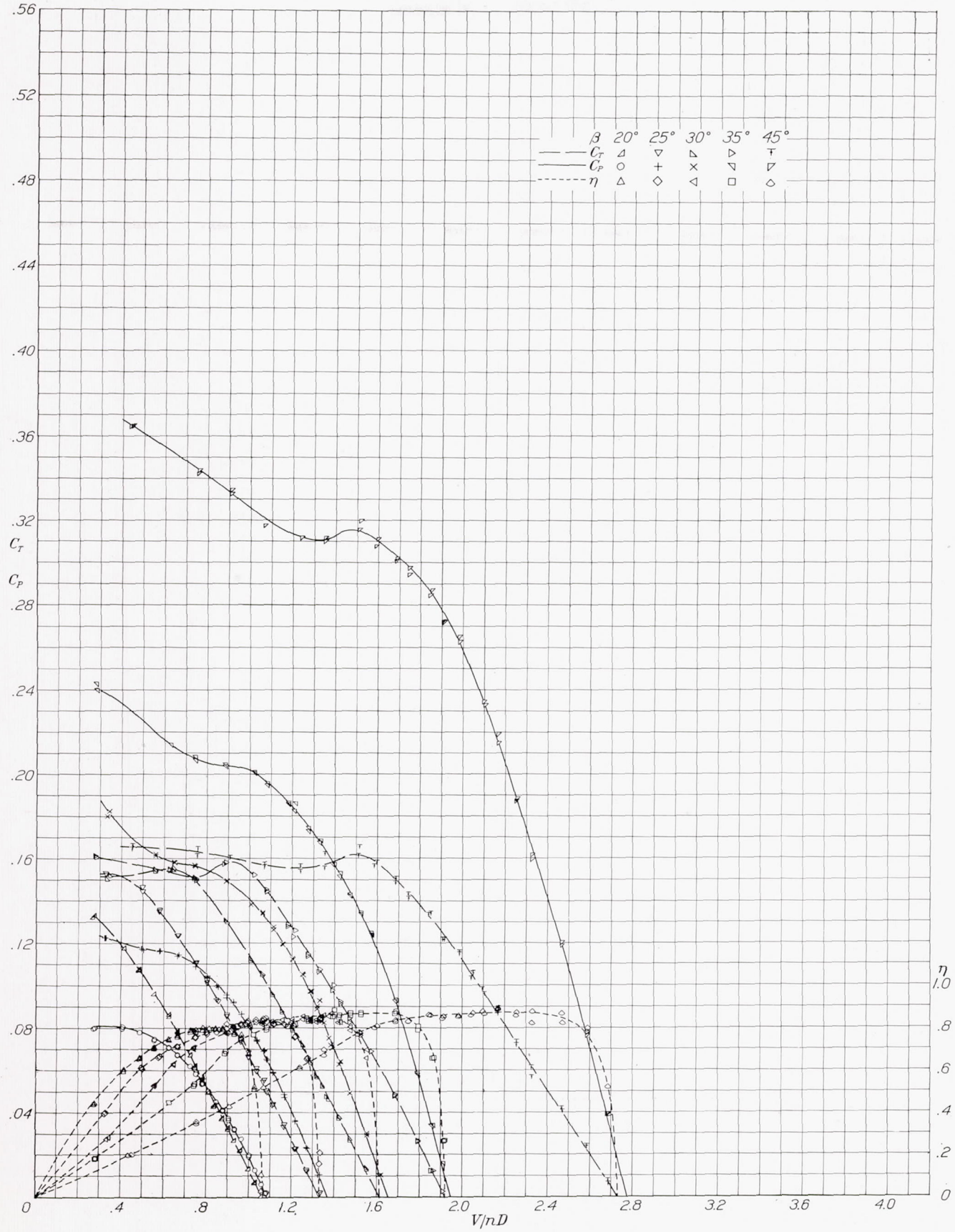

FIGURE 8.—Curves of C_T, C_P, and η against V/nD for propeller F on nose 1.

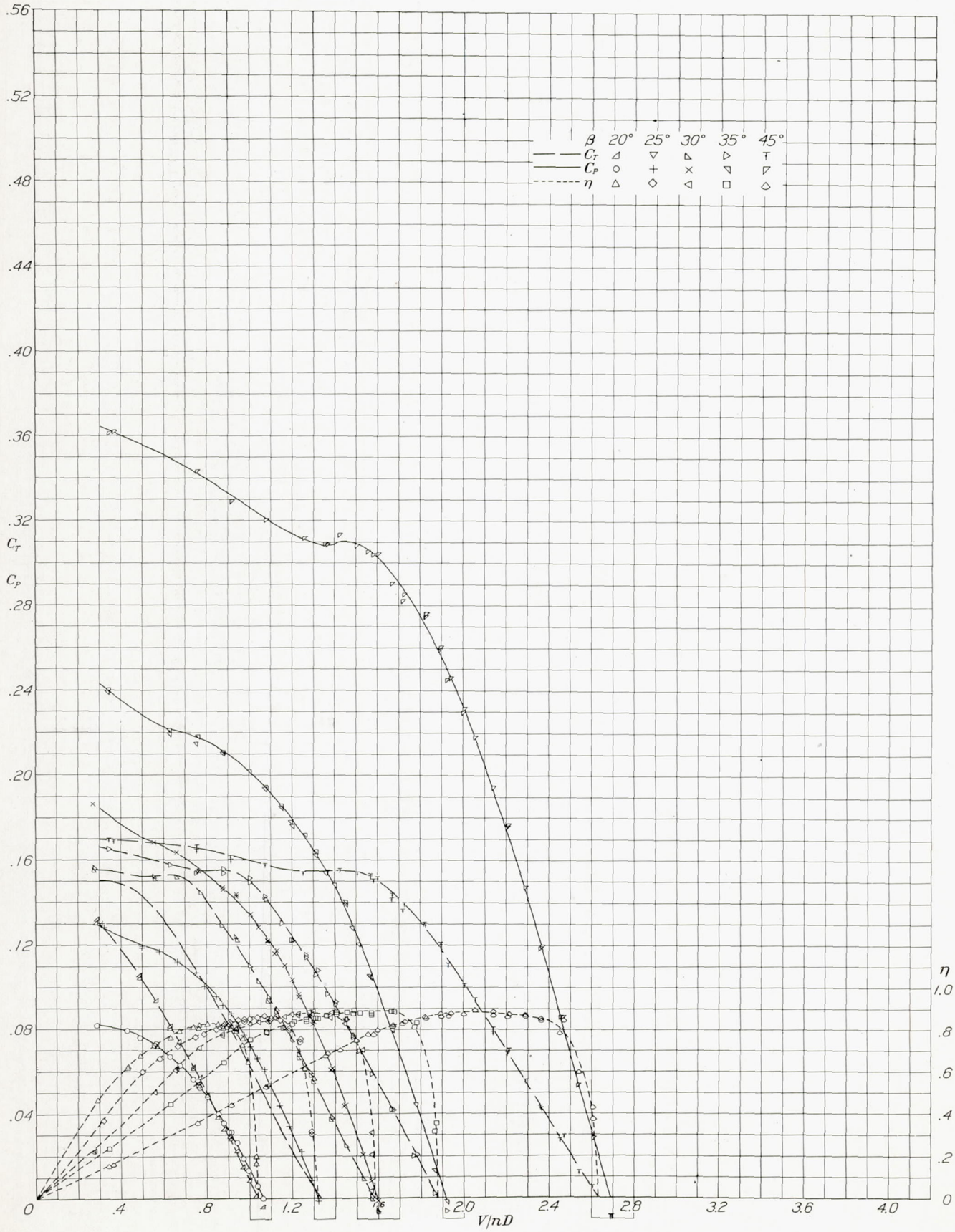

FIGURE 9.—Curves of C_T, C_P, and η against V/nD for propeller C on nose 1.

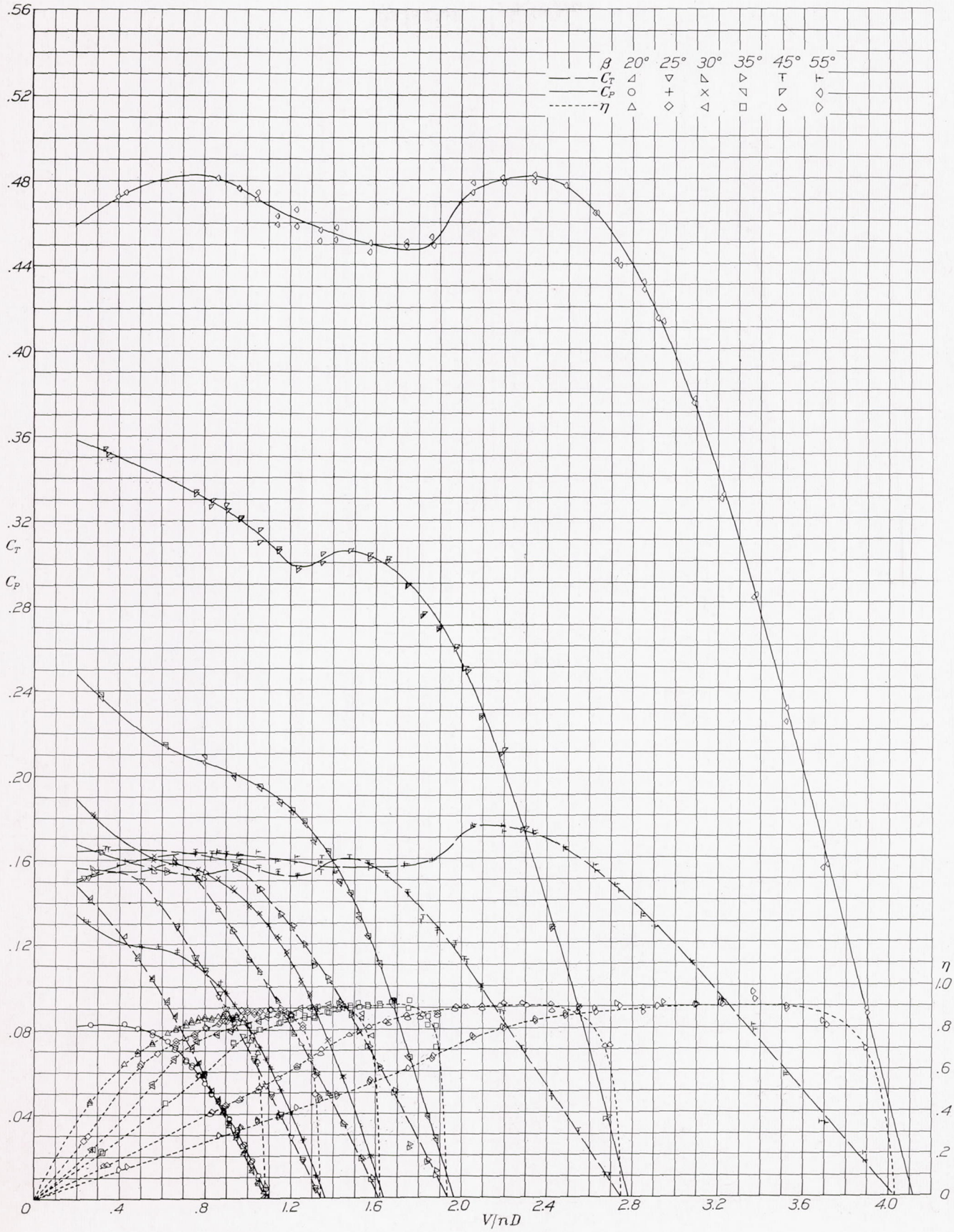

FIGURE 10.—Curves of C_T, C_P, and η against V/nD for propeller F on nose 3 with spinner 1.

325560—41——2

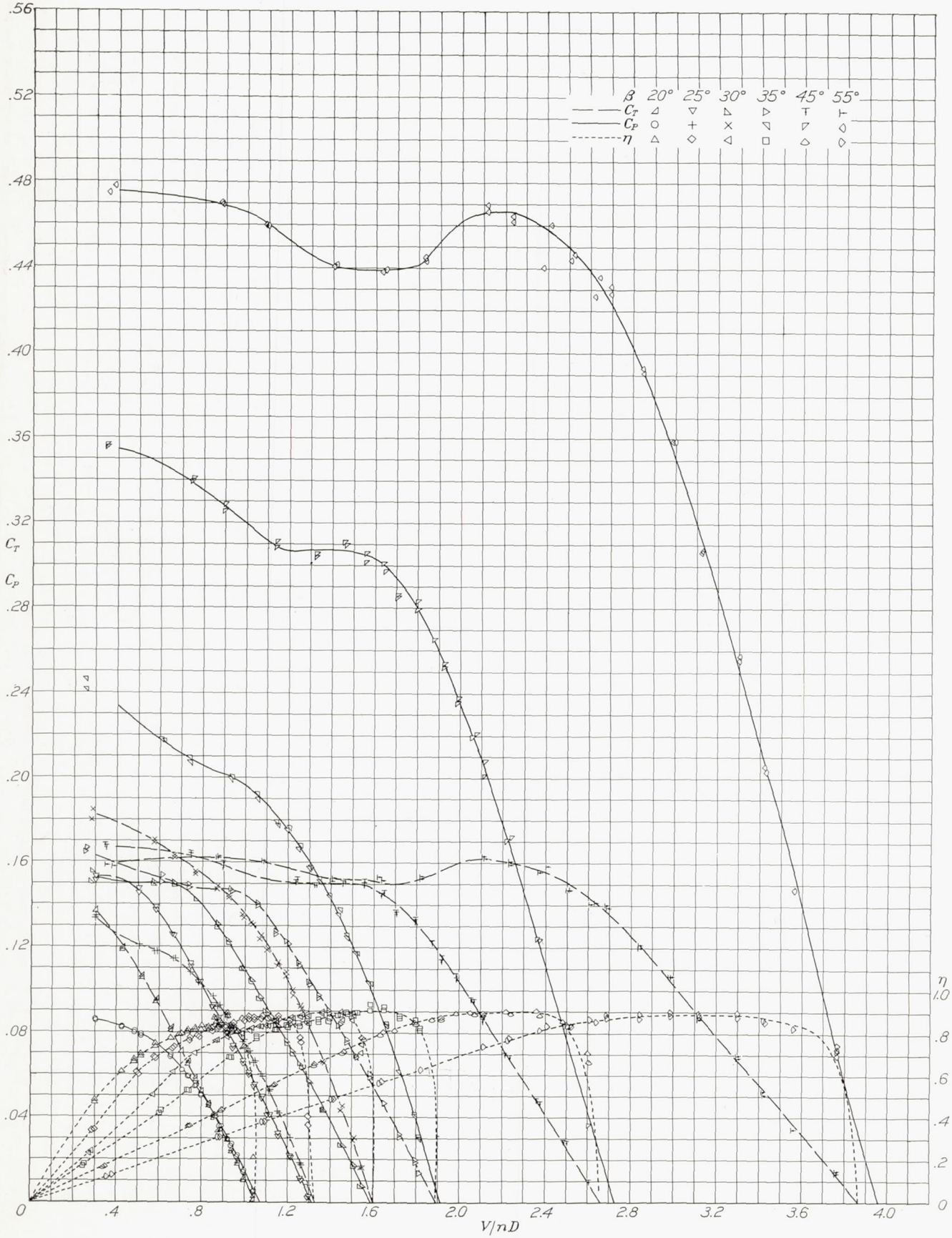

FIGURE 11.—Curves of C_T, C_P, and η against V/nD for propeller C on nose 3 with spinner 1.

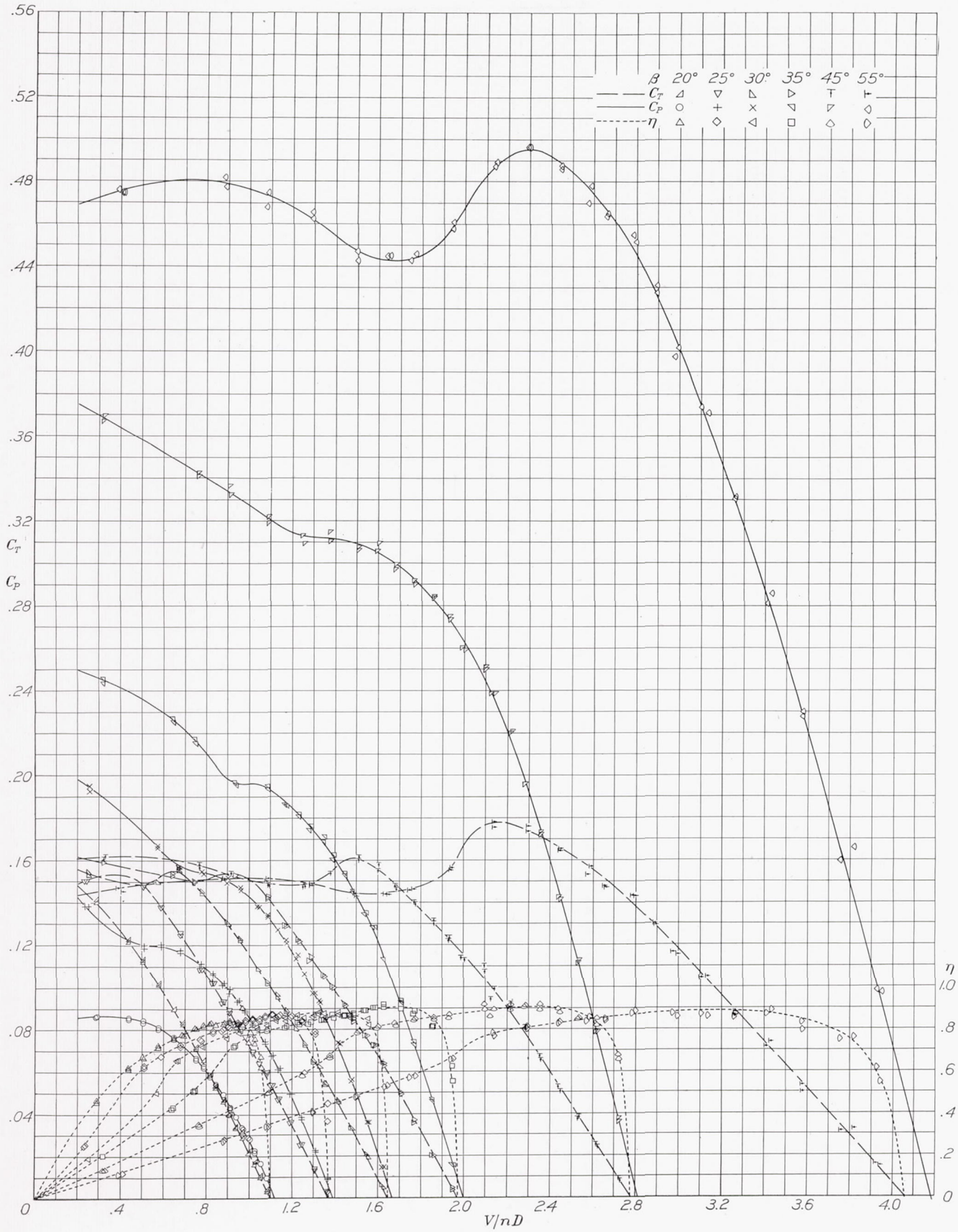

FIGURE 12.—Curves of C_T, C_P, and η against V/nD for propeller C_x on nose 3 with spinner 1.

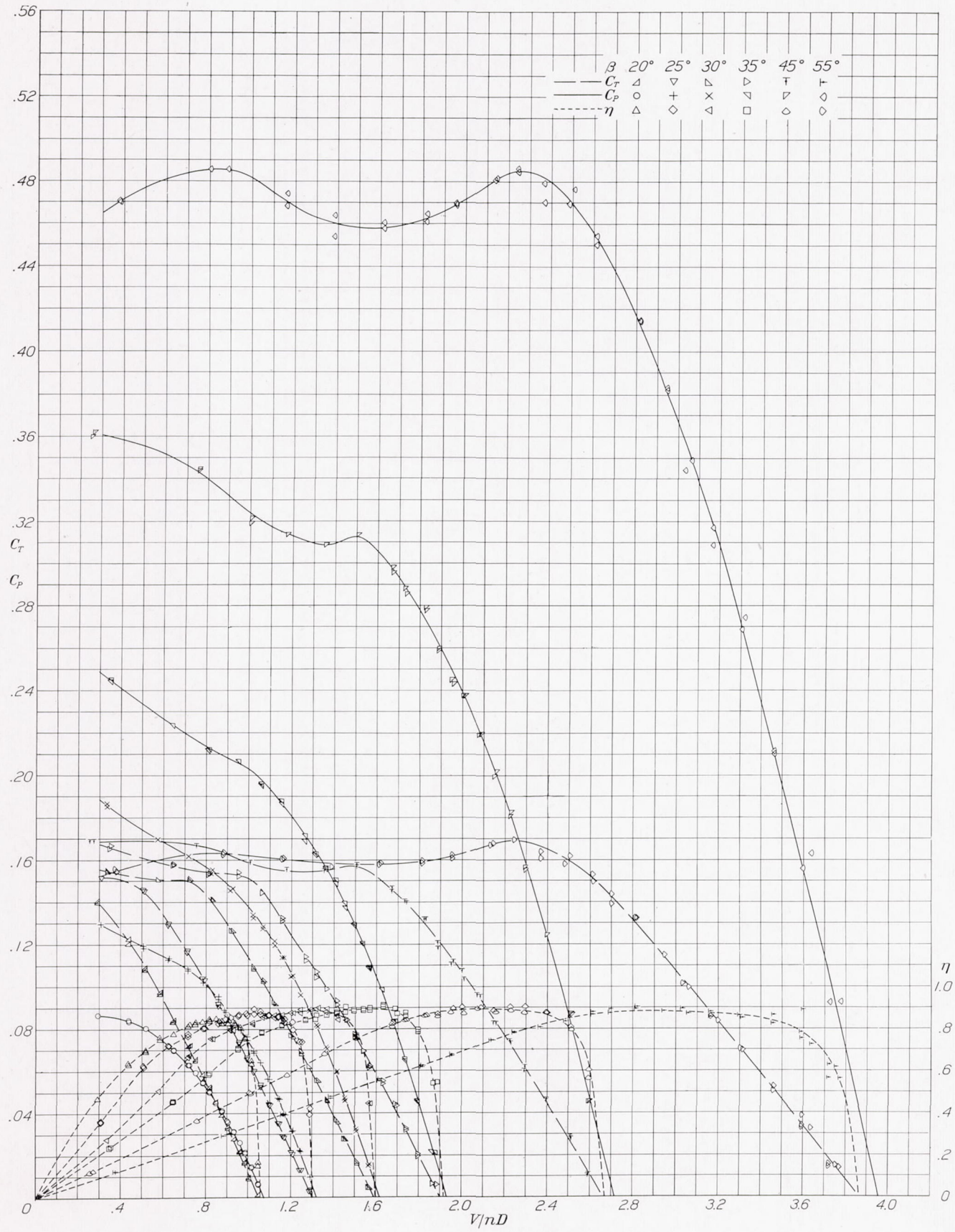

FIGURE 13.—Curves of C_T, C_P, and η against V/nD for propeller C on nose 4.

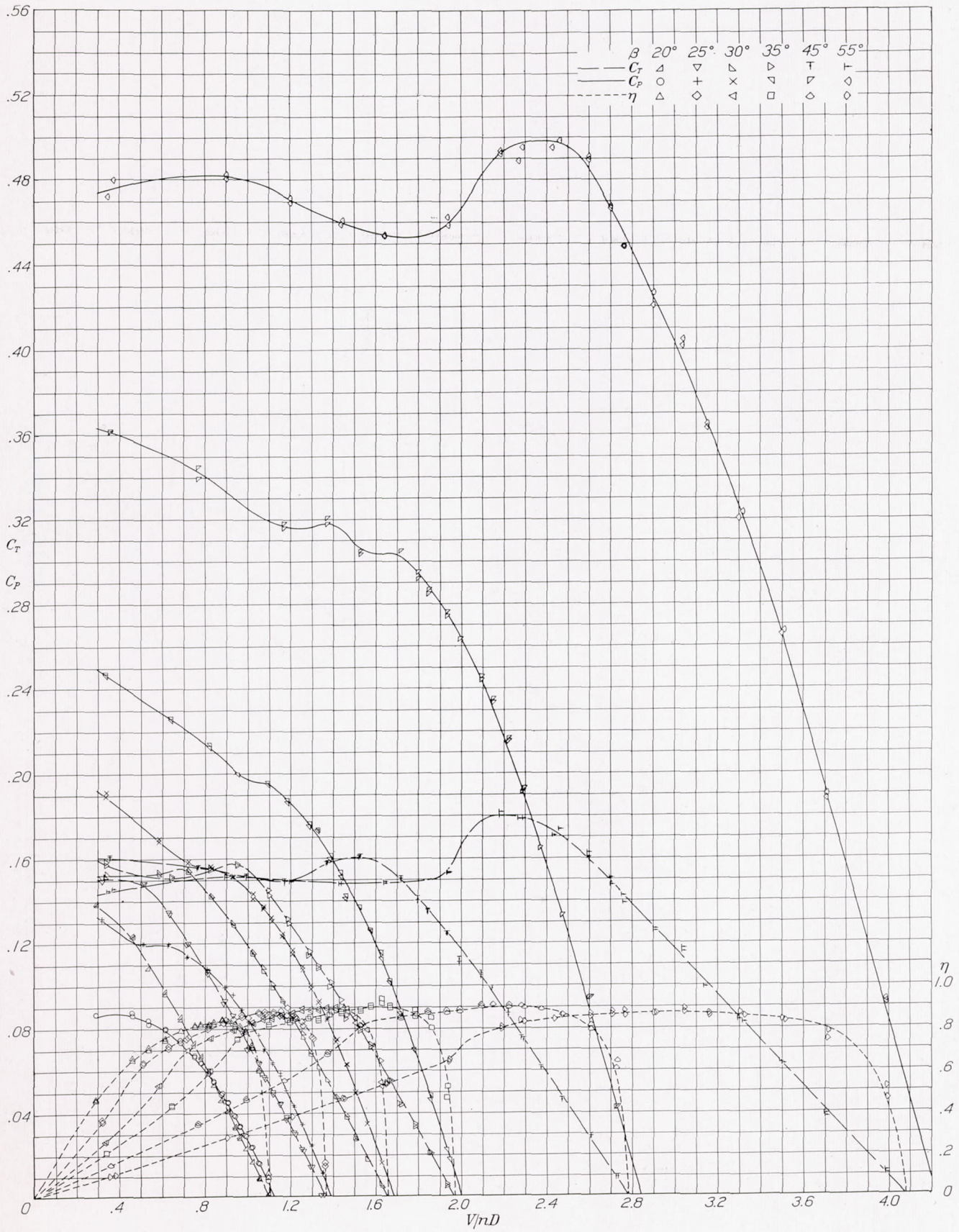

FIGURE 14.—Curves of C_T, C_P, and η against V/nD for propeller C_x on nose 4.

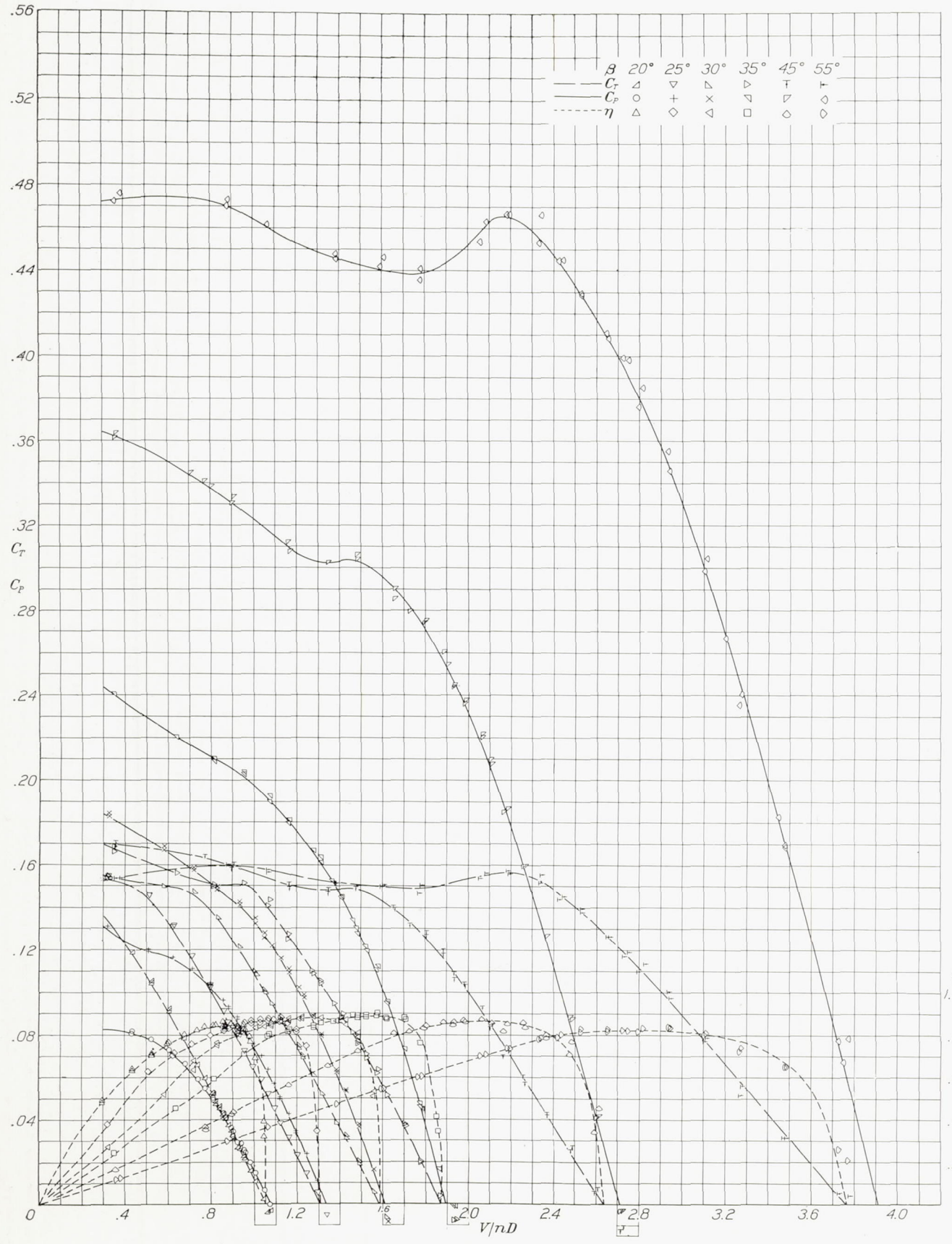

FIGURE 15.—Curves of C_T, C_P, and η against V/nD for propeller C on nose 5.

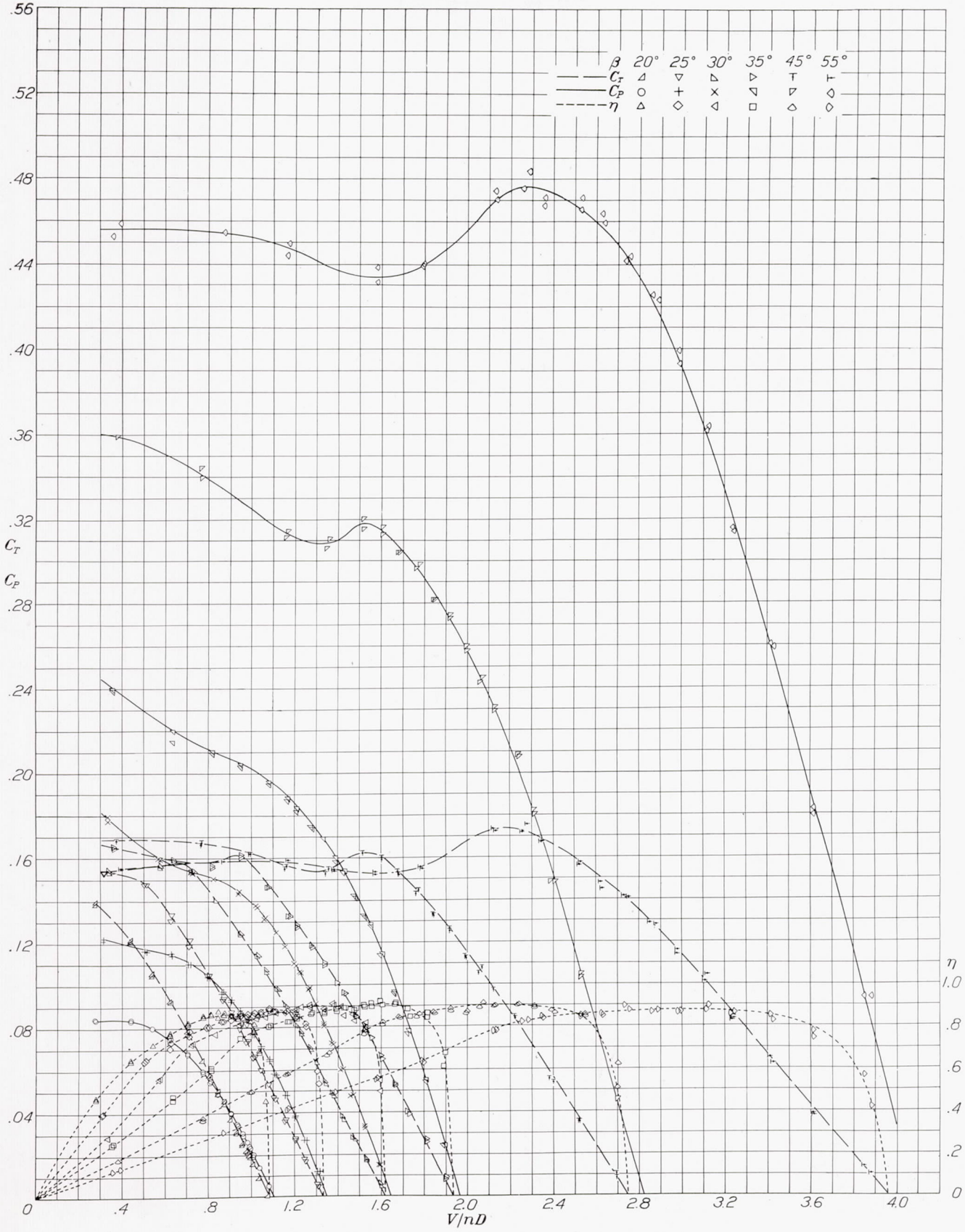

FIGURE 16.—Curves of C_T, C_P, and η against V/nD for propeller F on nose 5 with spinner 1.

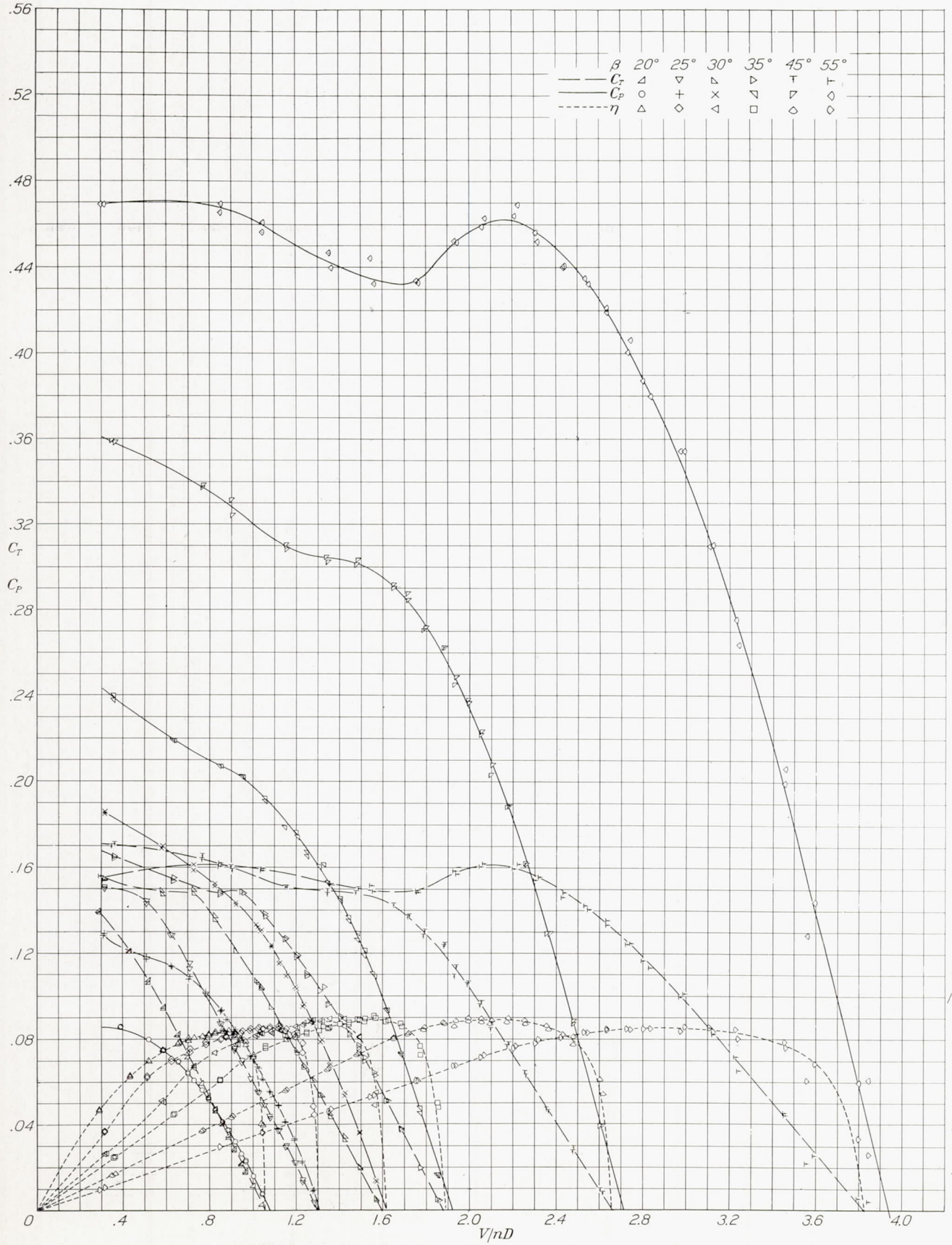

FIGURE 17.—Curves of C_T, C_P, and η against V/nD for propeller C on nose 5 with spinner 1.

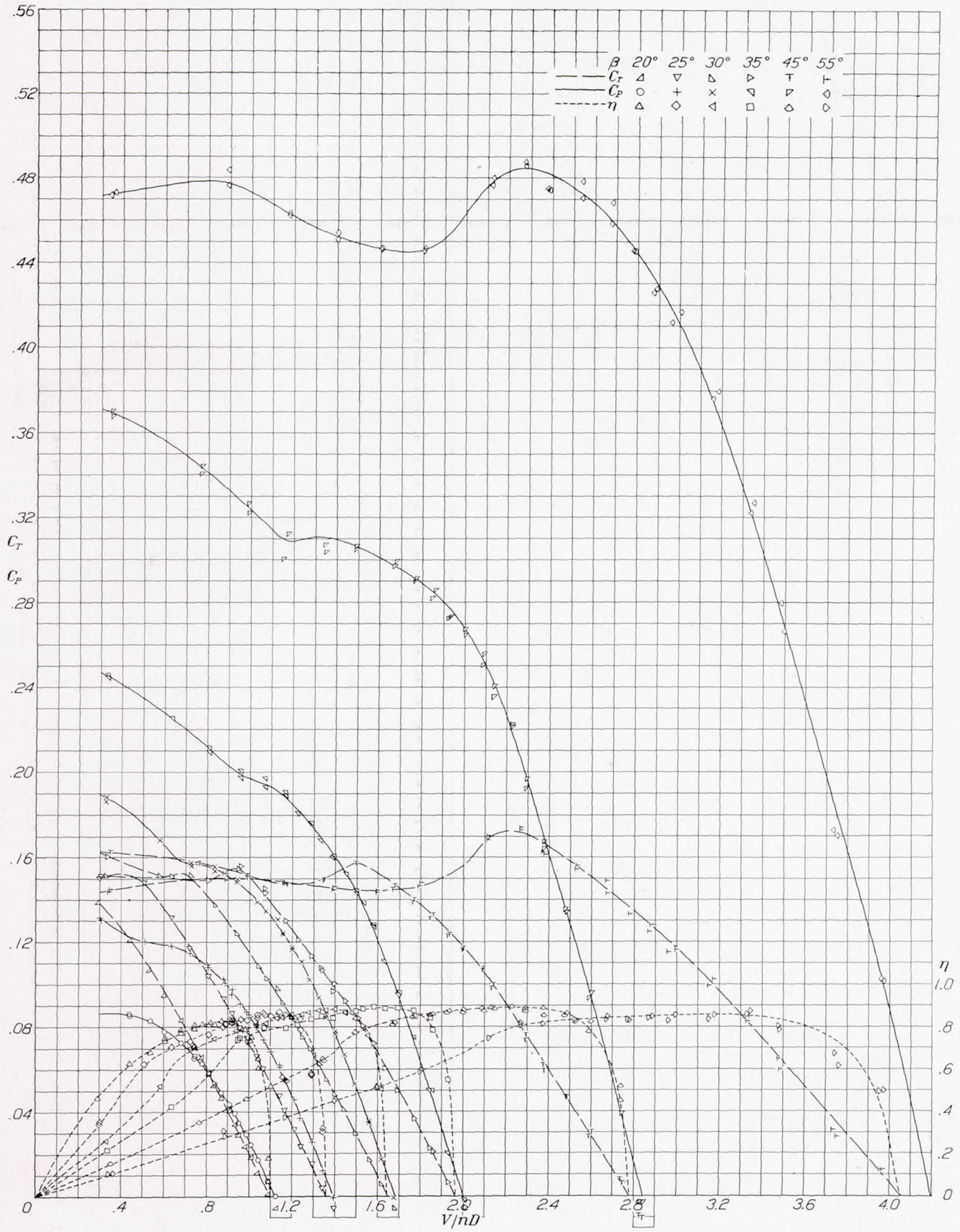

FIGURE 18.—Curves of C_T, C_P, and η against V/nD for propeller C_x on nose 5 with spinner 1.

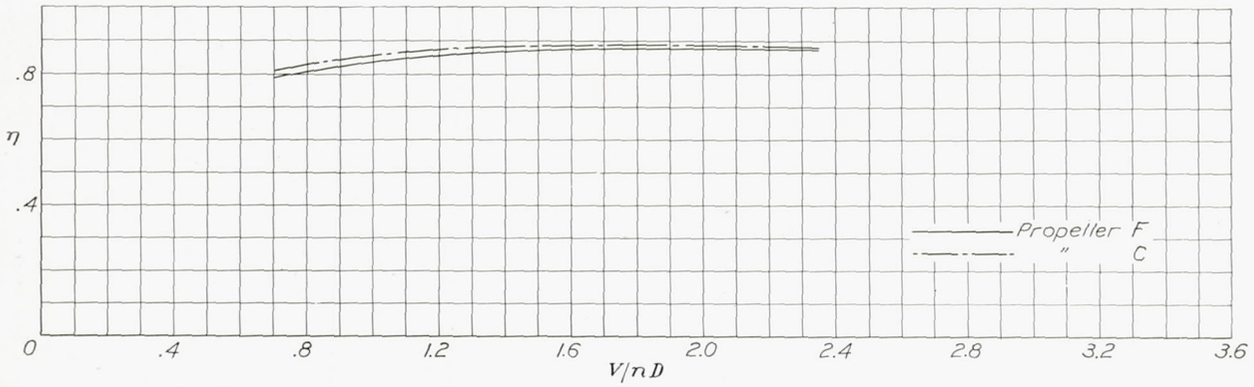

FIGURE 19.—Propulsive-efficiency envelopes against V/nD for propellers F and C on nose 1.

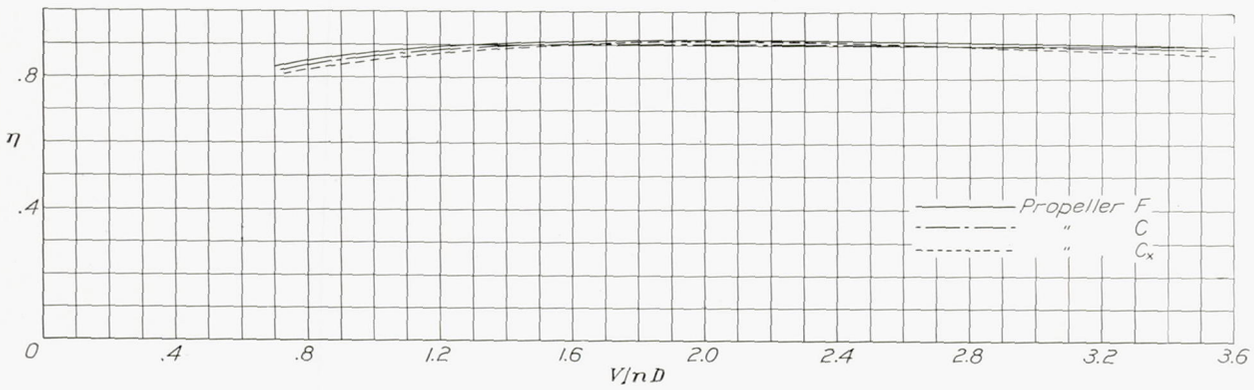

FIGURE 20.—Propulsive-efficiency envelopes against V/nD for propellers F, C, and C_x on nose 3 with spinner 1.

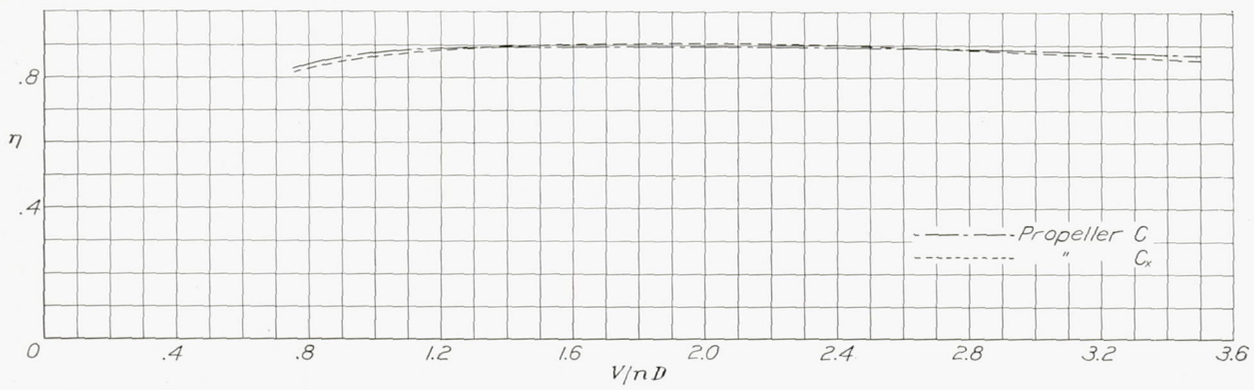

FIGURE 21.—Propulsive-efficiency envelopes against V/nD for propellers C and C_x on nose 4.

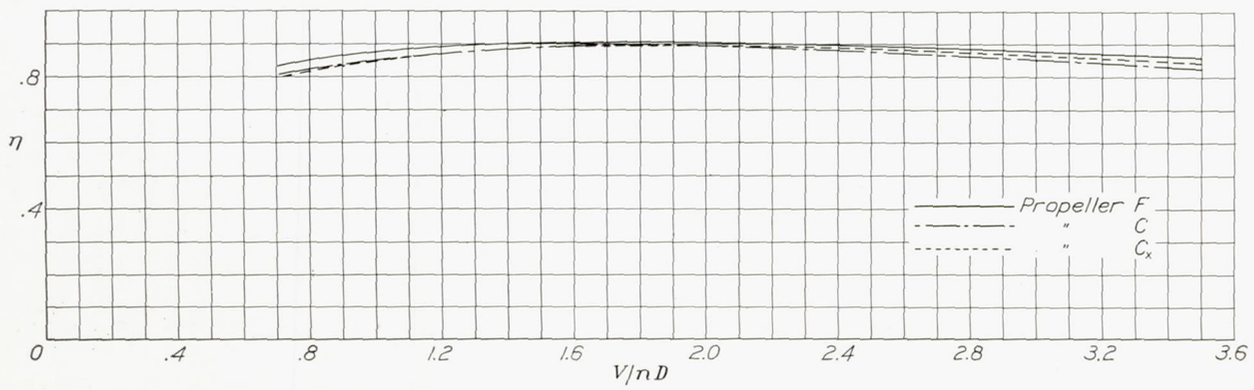

FIGURE 22.—Propulsive-efficiency envelopes against V/nD for propellers F, C, and C_x on nose 5 with spinner 1.

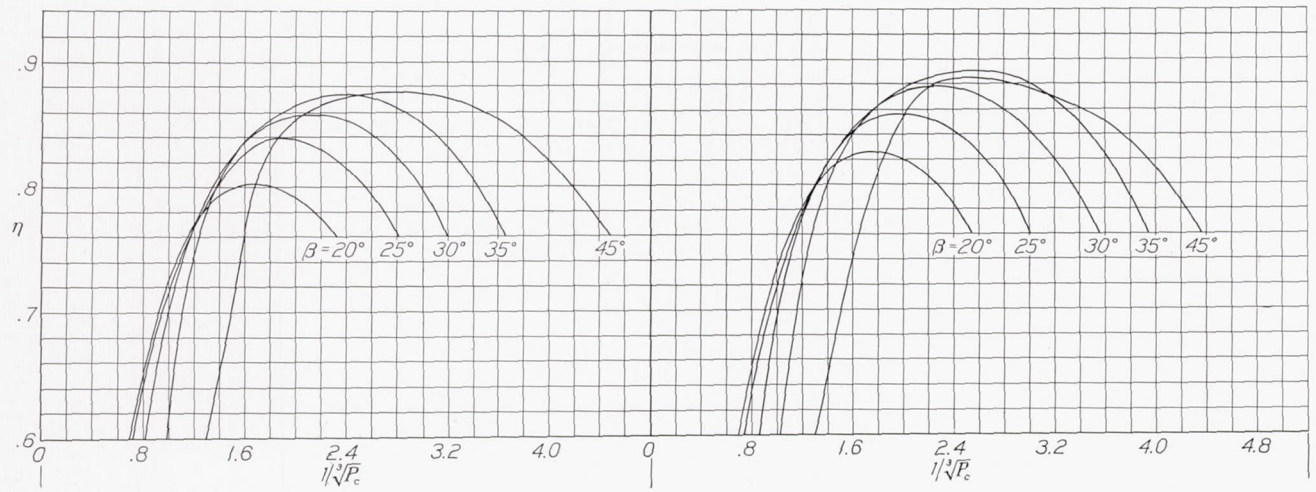

FIGURE 23.—Curves of propulsive efficiency against $1/\sqrt[3]{P_c}$ for propeller F on nose 1.

FIGURE 24.—Curves of propulsive efficiency against $1/\sqrt[3]{P_c}$ for propeller C on nose 1.

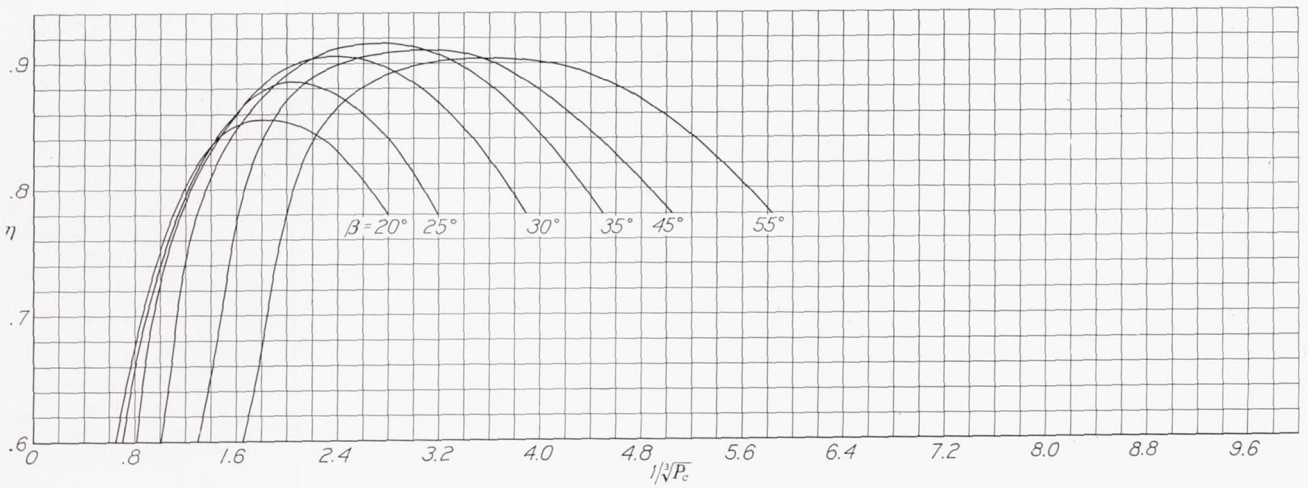

FIGURE 25.—Curves of propulsive efficiency against $1/\sqrt[3]{P_c}$ for propeller F on nose 3 with spinner 1.

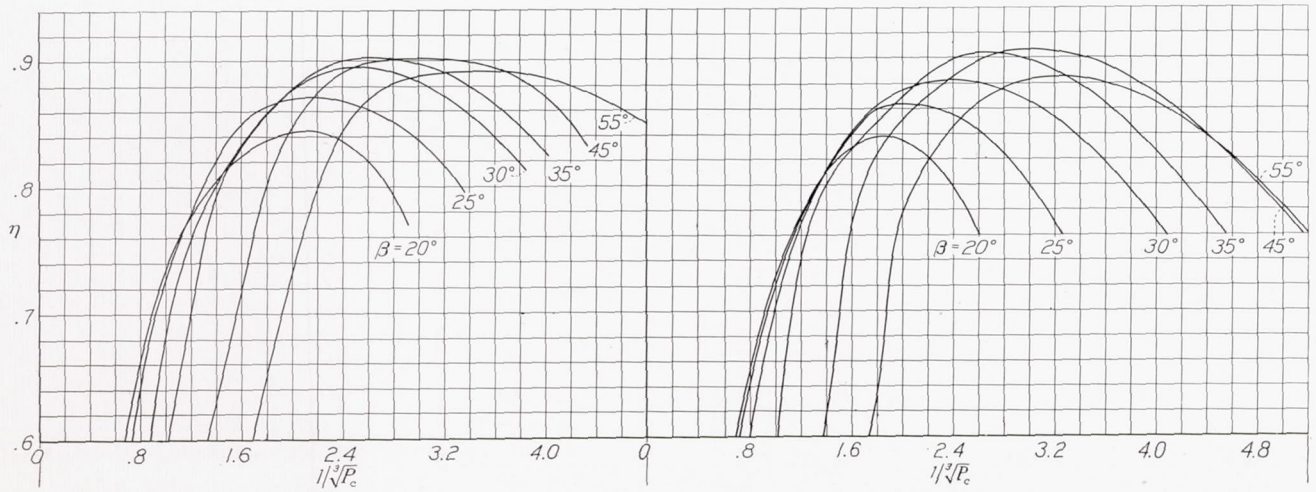

FIGURE 26.—Curves of propulsive efficiency against $1/\sqrt[3]{P_c}$ for propeller C on nose 3 with spinner 1.

FIGURE 27.—Curves of propulsive efficiency against $1/\sqrt[3]{P_c}$ for propeller C_x on nose 3 with spinner 1.

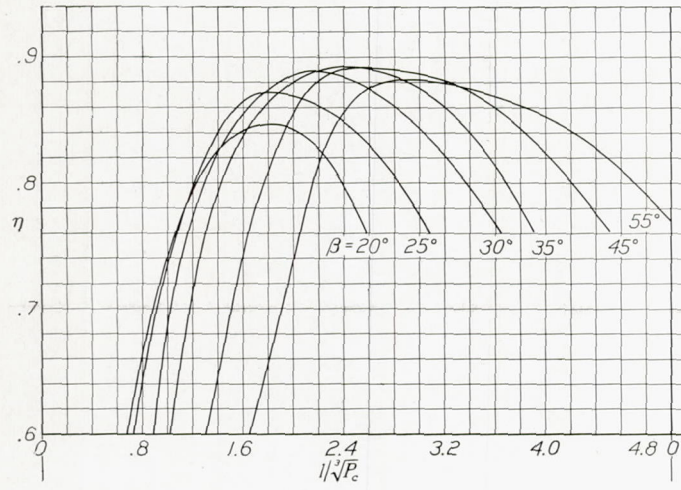

FIGURE 28.—Curves of propulsive efficiency against $1/\sqrt[3]{P_c}$ for propeller C on nose 4.

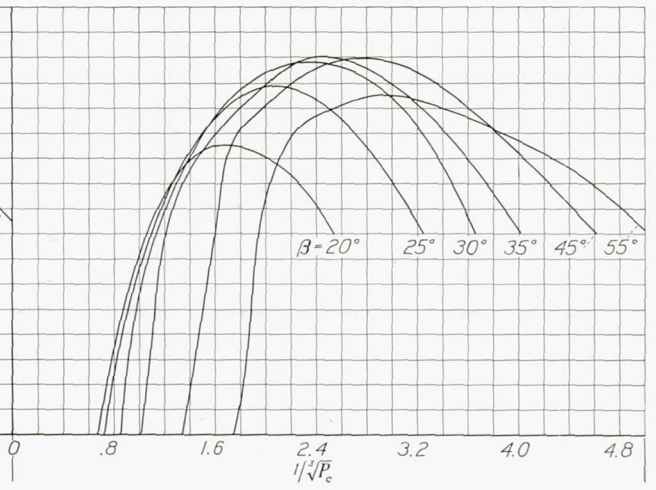

FIGURE 29.—Curves of propulsive efficiency against $1/\sqrt[3]{P_c}$ for propeller C_x on nose 4.

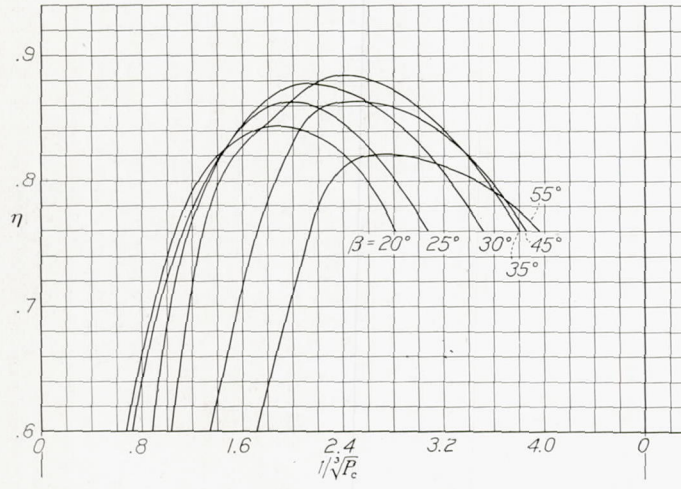

FIGURE 30.—Curves of propulsive efficiency against $1/\sqrt[3]{P_c}$ for propeller C on nose 5.

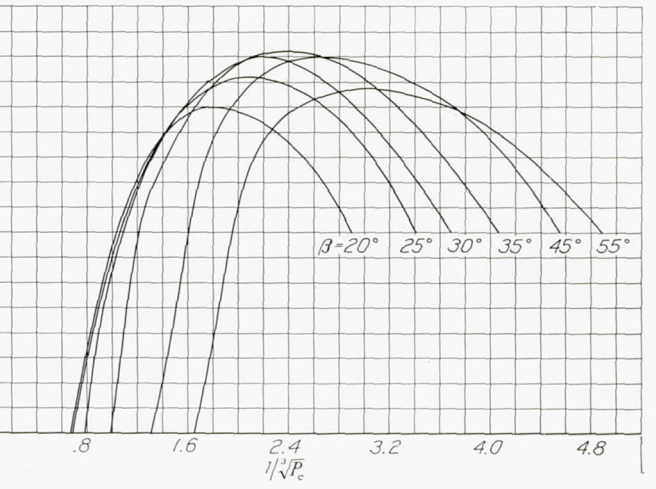

FIGURE 31.—Curves of propulsive efficiency against $1/\sqrt[3]{P_c}$ for propeller F on nose 5 with spinner 1.

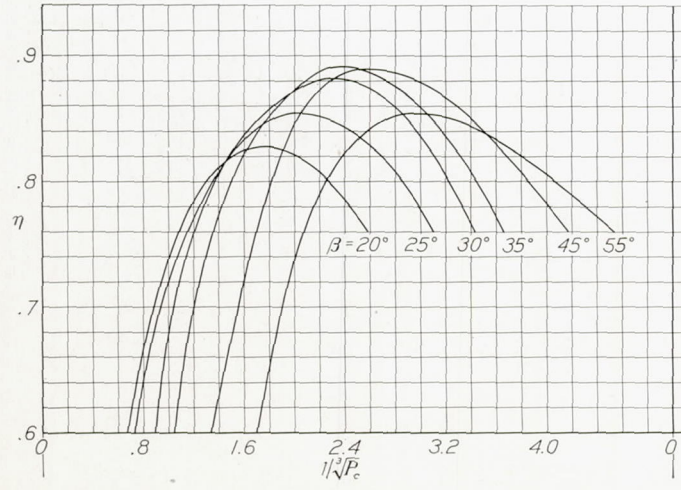

FIGURE 32.—Curves of propulsive efficiency against $1/\sqrt[3]{P_c}$ for propeller C on nose 5 with spinner 1.

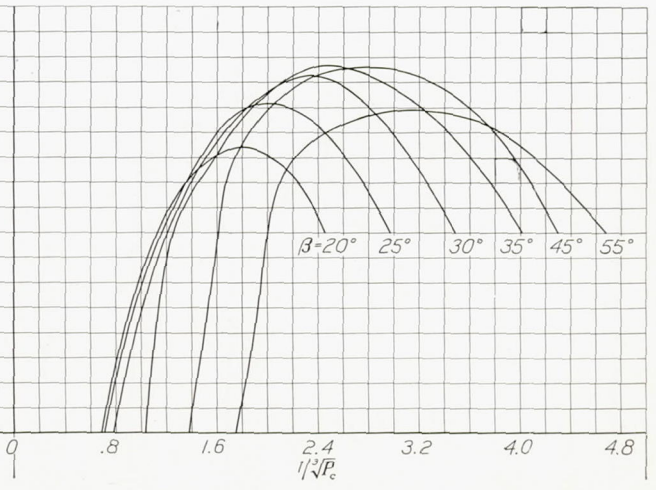

FIGURE 33.—Curves of propulsive efficiency against $1/\sqrt[3]{P_c}$ for propeller C_x on nose 5 with spinner 1.

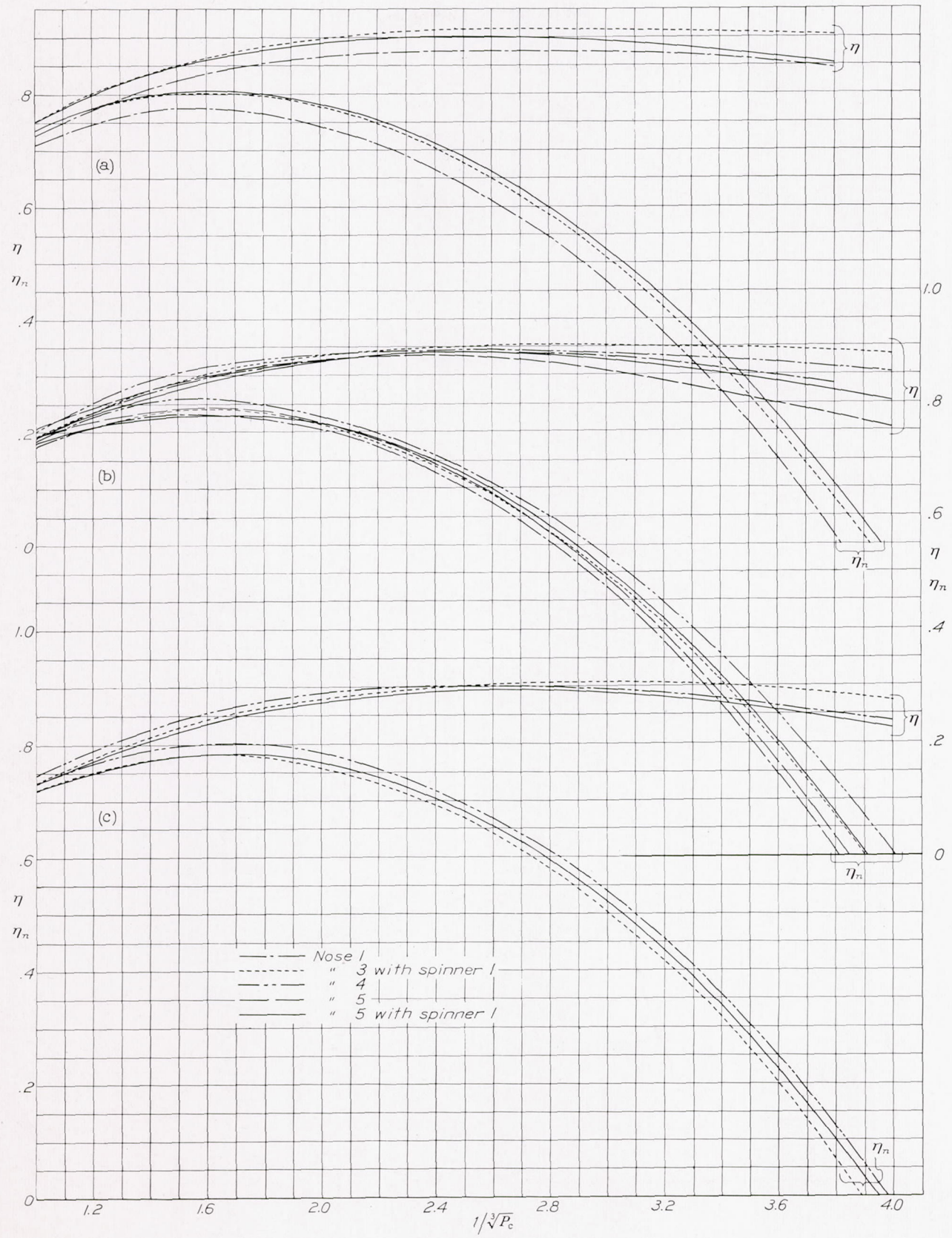

(a) Propeller F.
(b) Propeller C.
(c) Propeller C_x.

FIGURE 34.—Propulsive-efficiency and net-efficiency envelopes against $1/\sqrt[3]{P_c}$ for noses 1, 3, and 5.

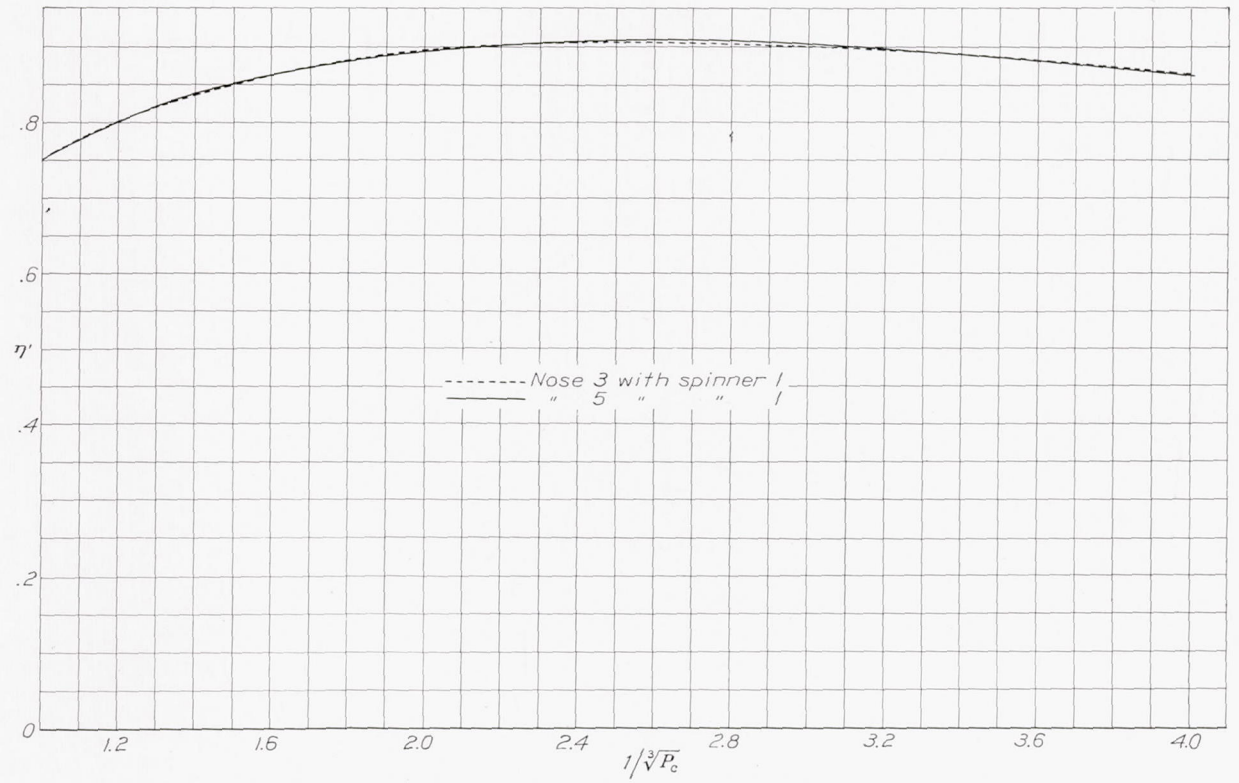

FIGURE 35.—Propulsive-efficiency envelopes against $1/\sqrt[3]{P_c}$ for propeller F on noses 3 and 5. (Spinner is considered as part of body.)

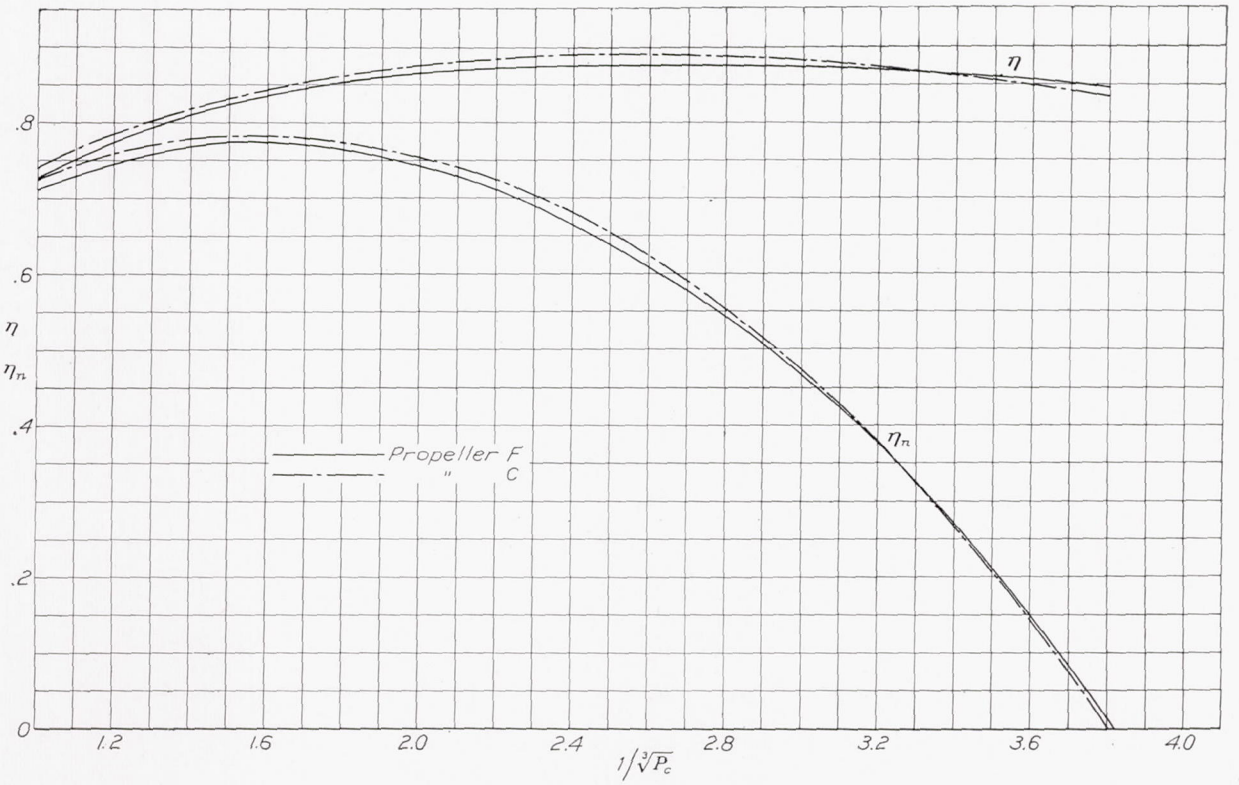

FIGURE 36.—Propulsive-efficiency and net-efficiency envelopes against $1/\sqrt[3]{P_c}$ for propellers F and C on nose 1.

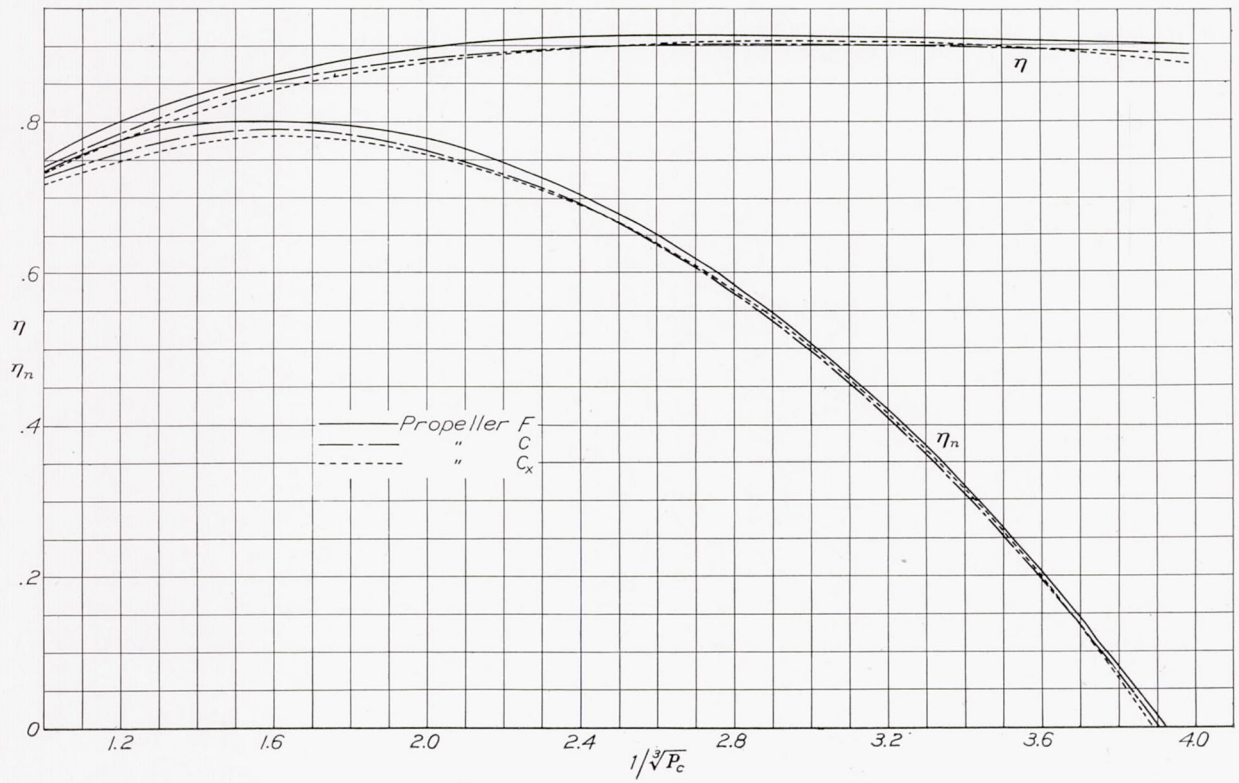

FIGURE 37.—Propulsive-efficiency and net-efficiency envelopes against $1/\sqrt[3]{P_c}$ for propellers F, C, and C_x on nose 3 with spinner 1.

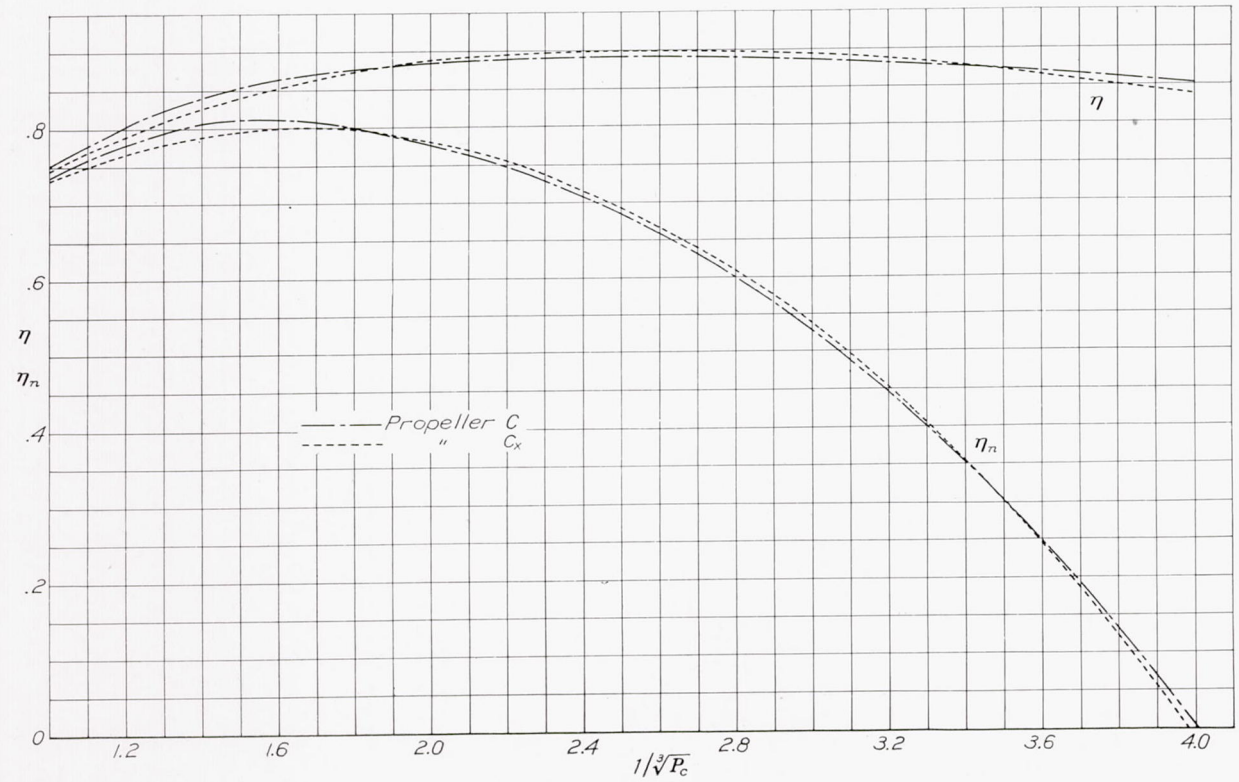

FIGURE 38.—Propulsive-efficiency and net-efficiency envelopes against $1/\sqrt[3]{P_c}$ for propellers C and C_x on nose 4.

DISCUSSION

The propulsive efficiency of the propeller was shown in reference 1 to be greatly dependent upon the shape of the body behind the propeller. This dependency is due to two main factors: (1) the effect of the slipstream in changing the drag of the body, and (2) the effect of the body in changing the angle of attack of the propeller sections. Reference 1 gives a good example of the radical change in drag of certain body shapes with the propeller-operating condition and of the consequent very high propulsive efficiency. The body shapes for the present report, however, are not subject to critical flow conditions; the drag due to the slipstream is therefore approximately proportional to the increase in dynamic pressure of the air over the body.

An estimate of the change in body drag due to the propeller slipstream can be made from an examination of the propulsive-efficiency curves plotted against $1/\sqrt[3]{P_c}$ in figures 23 to 33. The following table gives approximate average values, for all noses, of the factors entering into the computations of the increase in body drag due to the slipstream at peak propulsive efficiency for the 20° and the 55° blade-angle setting.

β (deg)	$1/\sqrt[3]{P_c}$	P_c	η	T_c	ΔD_P (percent)	ΔC_{D_P}	$\frac{\Delta C_{D_P}}{P_c}\frac{F}{S}$
20	1.6	0.244	0.80	0.195	19.5	0.0158	0.012
55	3.2	.0305	.88	.027	2.7	.00218	.013

The values of T_c give the average increase in dynamic pressure and therefore the percentage of increase in drag of the body ΔD_P, due to the propeller slipstream, if it is assumed that the flow increase is linear. For the 20° blade-angle setting, the drag increase amounts to approximately 20 percent and, for the 55° blade-angle setting, to approximately 3 percent of the body drag. The change in the drag coefficient ΔC_{D_P}, based on the drag coefficient of nose 1 (C_D=0.0809), is obtained by multiplying the percentage of change in ΔD_P by 0.0809. The difference between the propeller efficiency $\eta_P = TV/P$ and the propulsive efficiency $\eta = \frac{(T-\Delta D_P)\,V}{P}$ may be computed from the formula

$$\text{Change in efficiency} = \frac{\Delta C_{D_P}}{P_c}\frac{F}{S}$$

The values of the difference between propulsive and propeller efficiency are given in the last column of the table.

Now, because the maximum change in body drag due to the nose shape, that is, the change in drag from the open-nose cowling to the streamline nose, was only 12 percent and the change in drag due to the propeller slipstream for any of the noses tested caused a change in efficiency of only 1 percent, the relative change in efficiency with a change in nose shape is only 0.12 percent. The foregoing results show that the body drag has a negligible effect on relative comparisons of propulsive efficiency of a given propeller, unless critical flow conditions are encountered. The chief emphasis of this report is therefore confined to the second factor, the effect of the body in changing the angle of attack of the propeller sections.

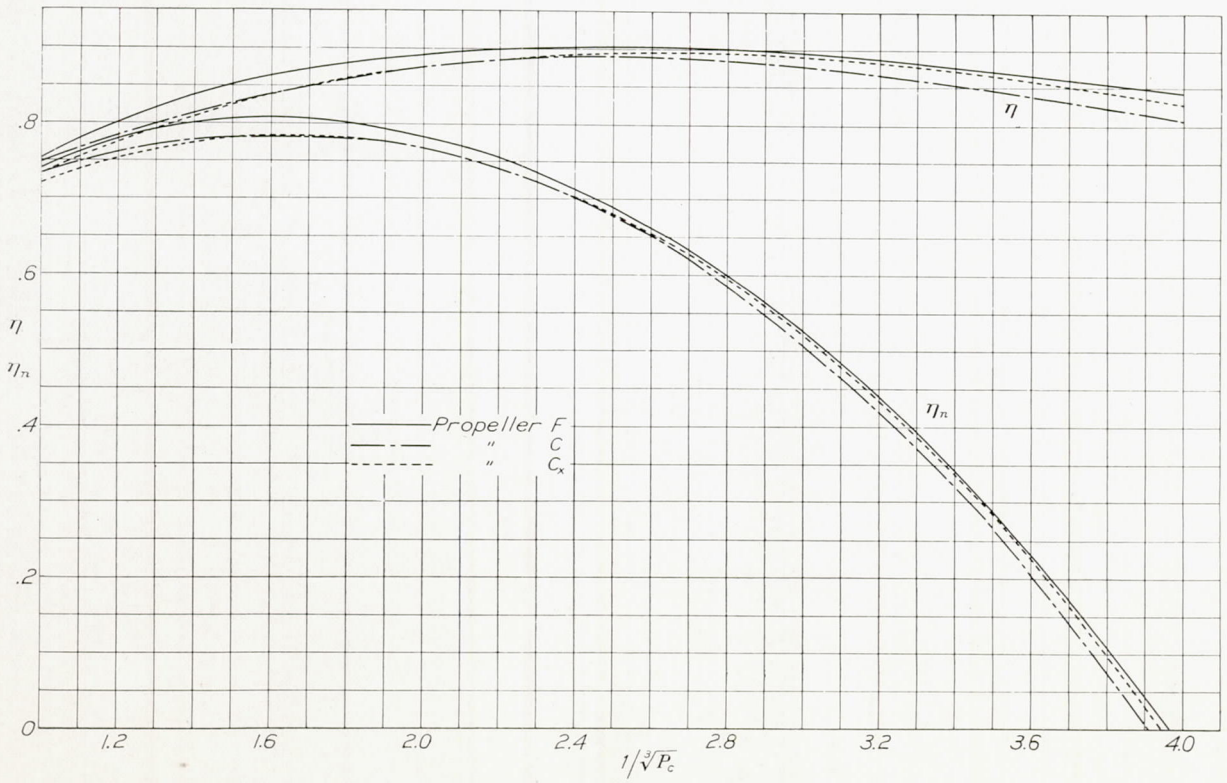

FIGURE 39.—Propulsive-efficiency and net-efficiency envelopes against $1/\sqrt[3]{P_c}$ for propellers F, C, and C_x on nose 5 with spinner 1.

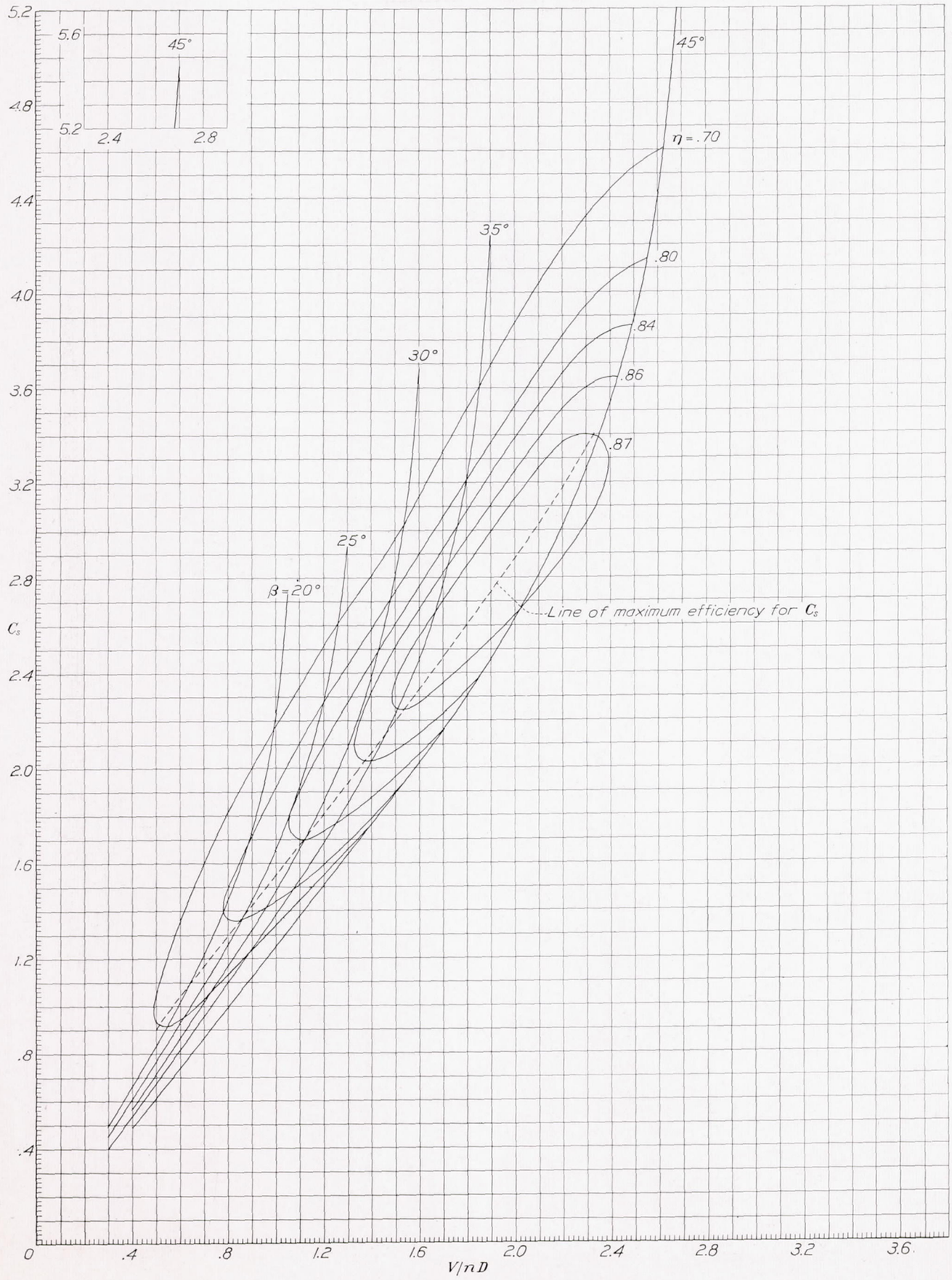

FIGURE 40.—Design characteristics for propeller F on nose 1.

FIGURE 41.—Design characteristics for propeller C on nose 1.

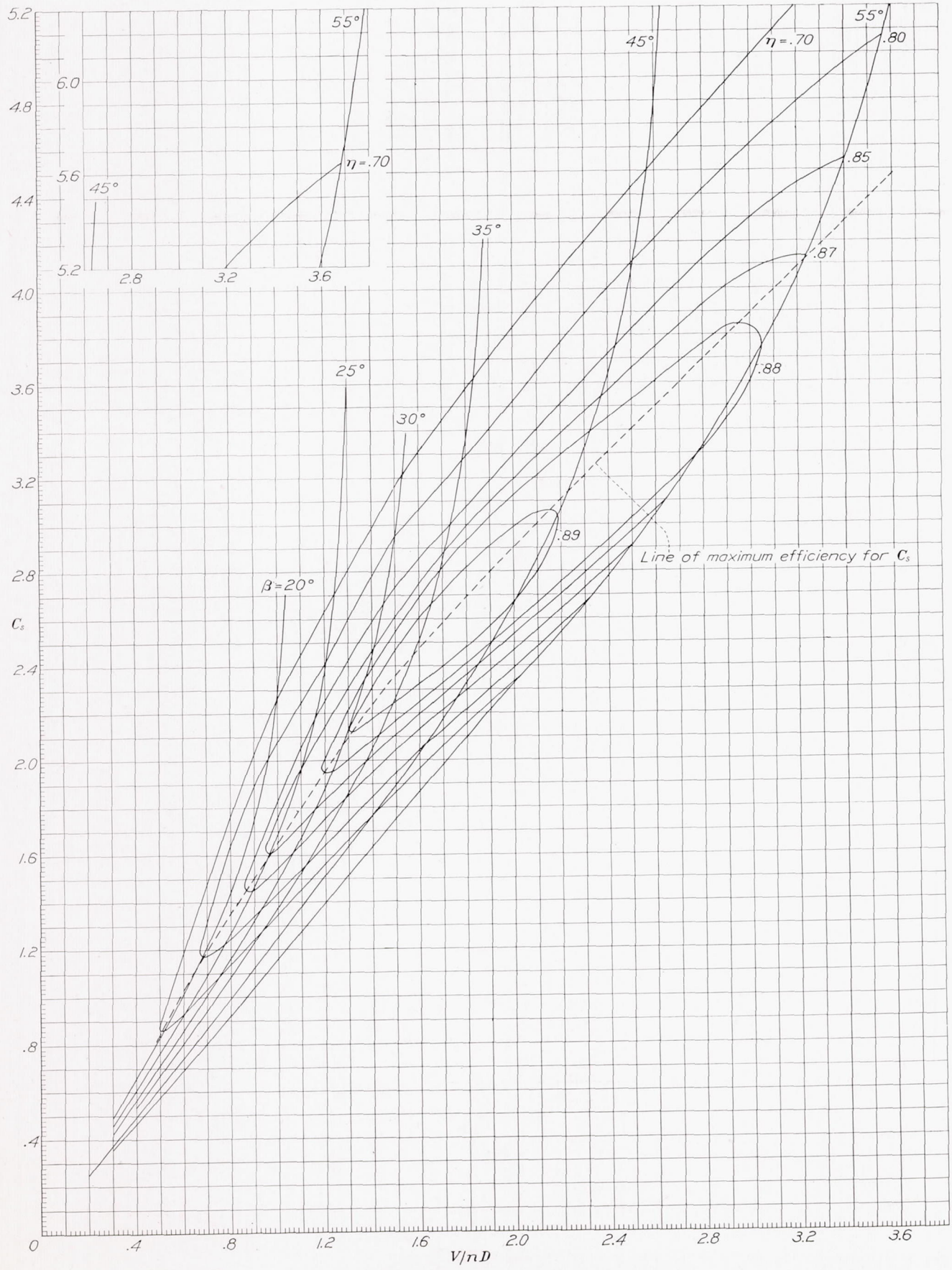

FIGURE 42.—Design characteristics for propeller C on nose 4.

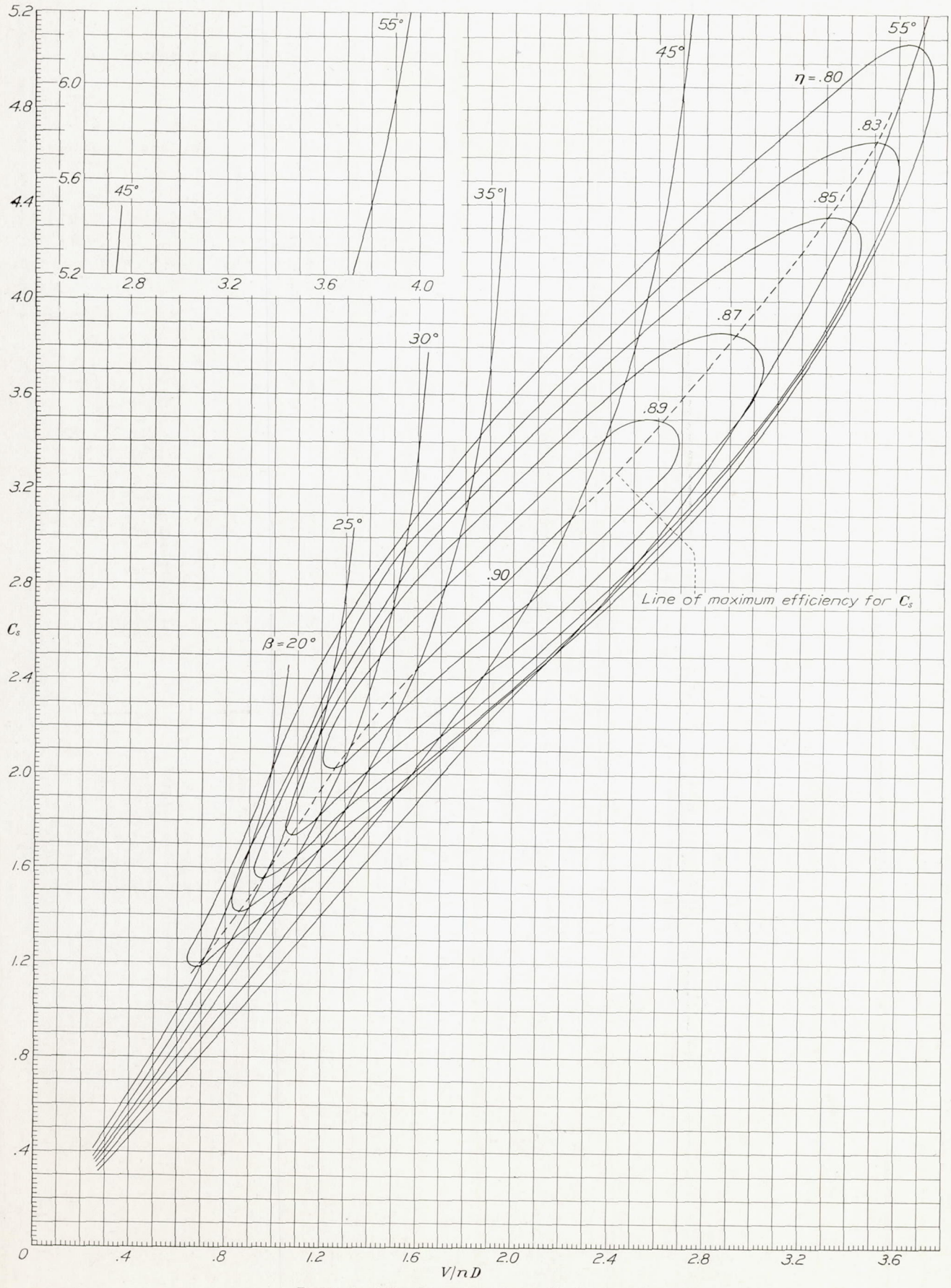

FIGURE 43.—Design characteristics for propeller C_x on nose 4.

If the interference velocities are neglected, the apparent angles of attack of the sections at any given value of V/nD may be computed from the pitch-distribution curves and the velocity distribution in the plane of the propeller with the propeller removed. Because of the difference in the aerodynamic characteristics of each section, it is desirable to refer the angle of attack to the zero-lift line. The angles of zero lift α_{a_0} for the sections of the three propellers are given in

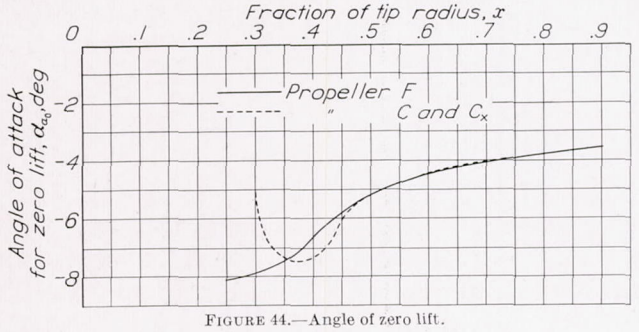

FIGURE 44.—Angle of zero lift.

figure 44. By the use of this figure, the apparent angles of attack above zero lift of the sections of propellers F, C, and C_x in front of noses 1, 4, and 5 with spinner 1 are given in figure 45 at V/nD for maximum efficiency. The velocity distribution in front of noses 4 and 5 was assumed to be uniform and equal to the free-stream velocity. The curves show the effect of the velocity distribution on the angles of attack of the propeller sections when the propeller was operating at peak efficiency. It should be noted that the low-velocity region in front of nose 1 causes a much higher angle of attack.

Before the discussion of the experimental results is given, it is desirable to summarize briefly the conclusions of propeller theory in regard to load distribution, as set forth by Glauert in reference 4. The observed results are then quite readily explained.

Optimum load distribution.—The simple momentum theory indicates that, for maximum efficiency, the axial-velocity distribution shall be independent of radius, that is, shall be of constant value across the wake. The general momentum theory, however, shows that this condition cannot be satisfied owing to the high angular velocities required near the axis. The required condition by the general momentum theory for the axial-velocity increase is that it shall be zero at the hub, increasing rapidly with radius for a short distance to an almost constant value for the remaining distance. The angular velocity has a maximum value at the hub and decreases outward. When the analysis is further modified to consider the effect of the finite number of blades, the velocities for the inner sections are only slightly modified but the axial and the rotational interference velocities rapidly decrease to zero in the neighborhood of the tip. When the analysis is again modified to include the effect of friction, the torque, and thereby the rotational velocities, is found to be increased for a given thrust.

Effect of shank section of propeller.—The effect of the shank section of a propeller may be considered in two parts: the blade sections and the pitch distribution. Propellers F and C have almost identical construction except for the section of the shank. Propeller F has airfoil sections extending much closer to the hub than propeller C, which, with round sections, is designed primarily for strength. The effect of this construction may be summarized as follows. At a value of $1/\sqrt[3]{P_c}$

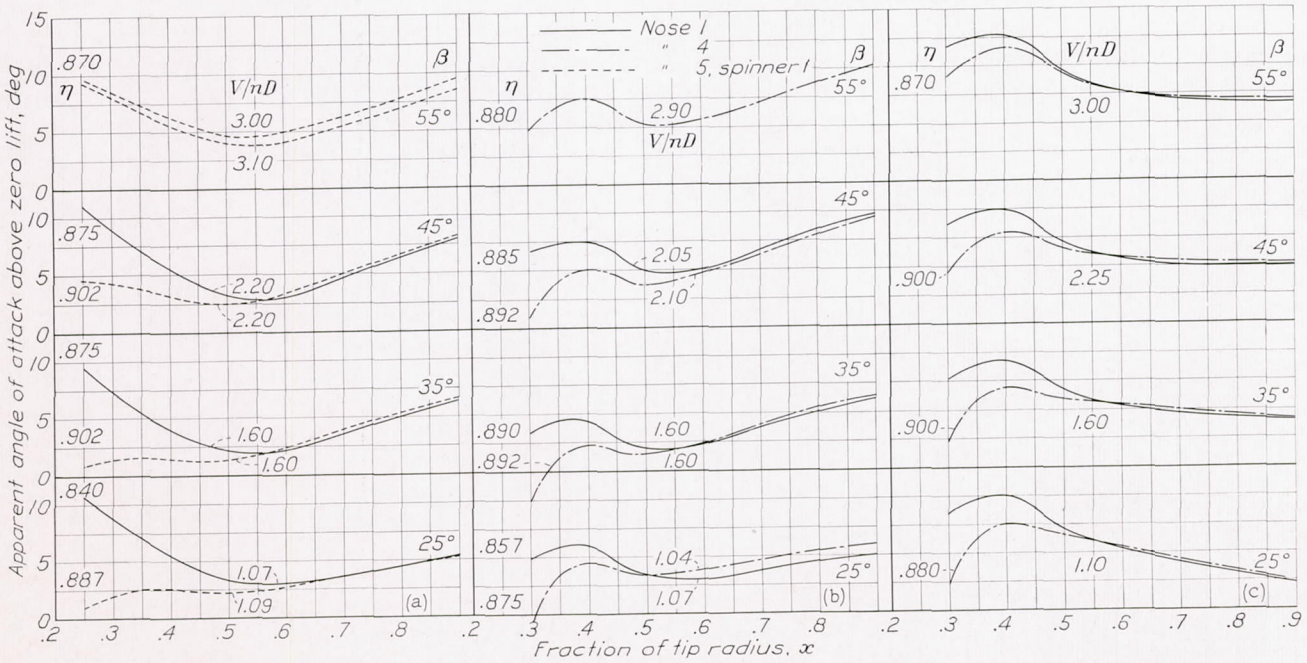

(a) Propeller F. (b) Propeller C. (c) Propeller C_x.

FIGURE 45.—Apparent angles of attack above zero lift of sections at V/nD for maximum efficiency.

of 2.6, a representative value for the high-speed condition of modern airplanes, the following propulsive efficiencies are obtained (figs. 23, 24, 31, and 32):

Propeller	Nose 1	Nose 5 spinner 1
F	87.5	90.3
C	89.0	89.0

The effect of the pitch distribution is obtained by the tests of nose 1 and nose 5 with spinner 1. A comparison of the angles of attack of the sections for propellers F and C ($\beta=35°$) in front of the two noses (figs. 45(a) and 45(b)) shows that the angle of attack increased from the 0.5 radius inward for nose 1 and decreased all the way to the hub for nose 5. As was stated in the preceding section, the ideal thrust and torque distribution is one that gives zero loading at the hub. Thus, the propellers operating in front of nose 5 have approximately the optimum conditions for maximum efficiency, that is, the smallest energy loss in the wake. The higher efficiency of propeller F is undoubtedly due to the better shape of the shank section, that is, an airfoil instead of a round shank shape.

In front of nose 1, the lower velocity air stream with its resulting high angle of attack causes a considerable increase in the loading for propeller F. (See fig. 45(a).) The values of the peak efficiencies are given to illustrate the loss incurred by overloading the inner sections of the propellers. This high loading is very detrimental to propeller F, causing about 3 percent loss in efficiency. The failure of propeller C to show any change in efficiency on noses 1 and 5 is undoubtedly due to two compensating effects. The shank sections are of such poor aerodynamic shape that, in the lower velocity region of nose 1, any loss due to increased load on the outer portion of the shank has apparently been neutralized by the reduced drag of the inner portion.

Propeller F might thus appear to be unfavorable for use in front of an open-nose NACA cowling. If the pitch of its inner sections is reduced, however, so as to obtain an optimum load distribution, propeller F should develop approximately the same efficiency as it does on nose 5. From cooling considerations, such a propeller would be very desirable in the low-speed range because it would give a considerable pressure boost on the front of the cowling owing to the positive angle of attack at a low value of V/nD.

Effect of spinner.—A comparison of the net and the propulsive efficiencies for propeller C in front of nose 5 with and without spinner 1 (fig. 34 (b)) illustrates the importance of covering the hub of the propeller when the velocity of the air stream is high. The advantage of the spinner is shown to increase as the disk loading is decreased, rising from 1 percent at $1/\sqrt[3]{P_c}=2.6$ to 5 percent at $1/\sqrt[3]{P_c}=4.0$. The importance of covering the hub becomes less significant when the propeller is operating in front of a blunt body such as nose 1, especially when the ratio of the hub diameter to the cowling diameter is small.

Effect of pitch distribution.—The effect of pitch distribution on the propeller performance may be seen by comparing the efficiencies of propellers C and C_x in the following table.

$1/\sqrt[3]{P_c}$	1.0			2.6			3.0		
Propeller	Nose 3	Nose 4	Nose 5	Nose 3	Nose 4	Nose 5	Nose 3	Nose 4	Nose 5
C	74.2	75.2	74.7	90.2	89.8	89.0	90.2	88.8	87.8
C_x	73.2	74.4	73.4	90.3	90.5	89.5	90.5	89.5	89.0
$\Delta\eta$	−1.0	−0.8	−1.3	0.1	0.7	0.5	0.3	0.7	1.2

Propeller C is seen to be the more efficient at the higher power loading corresponding to the climb condition ($1/\sqrt[3]{P_c}=1.0$) and propeller C_x is better in the high-speed-flight condition. These results are in accordance with theory, though the small differences would seem to be disappointing. Here again, however, the velocity pattern produced by the body affects the load distribution and thereby the efficiency.

Figures 45 (b) and 45 (c) give a comparison of the apparent angle of attack above zero lift for the propellers on noses 1 and 4. The principal defect of propeller C_x is that, owing to its method of construction, the pitch was not washed out on the inner sections. This construction is fairly satisfactory at low blade-angle settings for noses 4 and 5 with almost full velocity over these inner sections but, on nose 3 with its blocked flow, propeller C_x is only very little better than propeller C. The improvement obtained over the outer portion is almost nullified by the loss over the inner portion. This loss over the inner portion of the propeller becomes especially important at the 55° blade-angle setting. The angle of attack fails to decrease toward the hub, as is theoretically desirable. The resulting high loading on the inner region is probably the principal reason for the marked failure of the propellers when set 55° to reach peak efficiencies comparable with the 45° settings (figs. 27 and 29).

On noses 3 and 4 (figs. 37 and 38), the efficiency envelope for propeller C_x falls below that for propeller C at low power loadings ($1/\sqrt[3]{P_c}=3.7$, approximately). At this point, the excessive loading on the inner portion of propeller C_x is the probable reason for this difference. On nose 5 with spinner 1 (fig. 39), however, this crossing does not occur. The spinner may have caused a sufficient velocity increase to decrease the loading over the inner sections. In any event, this crossing occurs at power loadings beyond the peak efficiency for the 55° setting and would not be encountered in propeller design.

Propeller C_x was not tested on nose 1, but the curves for the apparent angles of attack of the sections have been included on the assumption that the maximum efficiency would occur at the same values of V/nD as

on nose 4. A small change in V/nD would have no effect on the general trend of the curves but would simply shift the whole curve up or down. The apparent angles of attack for two values of V/nD have been included (fig. 45 (a)) for propeller F in front of nose 5 with spinner 1 to show the effect of V/nD on the trend of the curve. A study of the curves for propellers C and C_x on nose 1 (fig. 45 (b) and 47 (c)) indicates that propeller C would be superior over the entire range because the inner sections of propeller C_x would be overloaded. This probable increased loading on the inner sections of propeller C_x may explain the result reported in reference 2, in which propeller C was found to be superior to propeller C_x over the entire high-speed-flight range.

Application to propeller design.—The propeller, as actually constructed, is always a compromise between the aerodynamic and the structural requirements. Aerodynamically, the propeller near the axis should consist of small streamline sections working at a low lift coefficient. Structurally, this form would be impossible because of the engine shaft, the hub providing blade support, and the mechanism for pitch variation. For minimum loss, these parts should be enclosed in a suitable spinner. Aerodynamically, the working portion of the blade should consist of sections having a high maximum value of lift-drag ratio. The section should be set at the proper working angle for maximum lift-drag ratio, and the chord should be just large enough to secure the desired loading. Again, this design cannot be realized structurally because such a small-chord propeller would be impracticable owing to vibration and flutter. When the propeller is structurally sound, any attempt to set the pitch in such a way as to secure maximum lift-drag ratio results in a power loading great enough to give excessive momentum losses in the wake. Thus, it is seen that a propeller section works below the maximum lift-drag ratio. From the foregoing discussion, it is concluded that the low-solidity, two-blade propeller is more efficient than the higher-solidity, three-blade and four-blade propellers because the two-blade propeller is more heavily loaded per blade, bringing it nearer the maximum lift-drag ratio.

It thus appears that the only possibilities for improvement in the propeller lie in the choice of the profile section and the pitch distribution. The importance of pitch distribution increases with V/nD. At low speed, that is, low values of V/nD, the pitch distribution is of secondary importance. Under these circumstances, the rotational-energy loss is a very small proportion of the total-energy loss, and nearly optimum conditions are easily secured. At high values of V/nD, however, the pitch distribution becomes important. In the operating region corresponding to a propeller setting of 45° at 0.75 R, for optimum conditions the rotational-energy and the axial-energy losses are approximately equal. These energy losses may be computed by the method outlined in reference 5. Alterations of the load distribution on the outer portion of the propeller have little effect upon the proportion of rotational and axial losses, but an excessive loading on the inner portion can easily make the rotational-energy loss several times the axial loss. At this operating condition, it is essential that proper consideration be given to the local velocity (due to body blocking) in the design of the pitch distribution.

CONCLUSIONS

The ideal plan form of the propeller cannot be attained because of structural requirements. These requirements demand a propeller chord too large to be efficiently operated at the maximum lift-drag ratio of the propeller section. With the plan form and the chord fixed, the problem of obtaining optimum load distribution becomes one of selection of the pitch distribution. The results show that:

1. In the design of the pitch distribution, it is essential that proper consideration be given to the velocity field produced by the presence of the body adjacent to the propeller.

2. The presence of a body behind the propeller produces its chief effect on the inner sections of the propeller blades.

   (*a*) When the inner sections are of conventional round-shank design, the important effect is the change in the drag of these sections due to the reduced velocity in front of the body.

   (*b*) When the inner sections are of a good airfoil design, the main effect is the change of the load distribution of the propeller due to increasing the angle of attack by reduction of the forward velocity.

3. The gain in efficiency realized by covering the propeller hub with a spinner is a function of the local velocity to which the hub is exposed, and the possible gain increases as the power loading decreases.

LANGLEY MEMORIAL AERONAUTICAL LABORATORY,
NATIONAL ADVISORY COMMITTEE FOR AERONAUTICS,
LANGLEY FIELD, VA., *January 29, 1940.*

REFERENCES

1. Theodorsen, Theodore, Stickle, George W., and Brevoort, M. J.: Characteristics of Six Propellers Including the High-Speed Range. Rep. No. 594, NACA, 1937.
2. Biermann, David, and Hartman, Edwin P.: Tests of Two Full-Scale Propellers with Different Pitch Distributions, at Blade Angles up to 60°. Rep. No. 658, NACA, 1939.
3. Weick, Fred E., and Wood, Donald H.: The Twenty-Foot Propeller Research Tunnel of the National Advisory Committee for Aeronautics. Rep. No. 300, NACA, 1928.
4. Glauert, H.: Airplane Propellers. Vol. IV, div. L of Aerodynamic Theory, W. F. Durand, ed., Julius Springer (Berlin), 1935, pp. 169–360.
5. Stickle, George W., and Crigler, John L.: Propeller Analysis from Experimental Data. Rep. No. 712, NACA, 1941.

U. S. GOVERNMENT PRINTING OFFICE: 1942

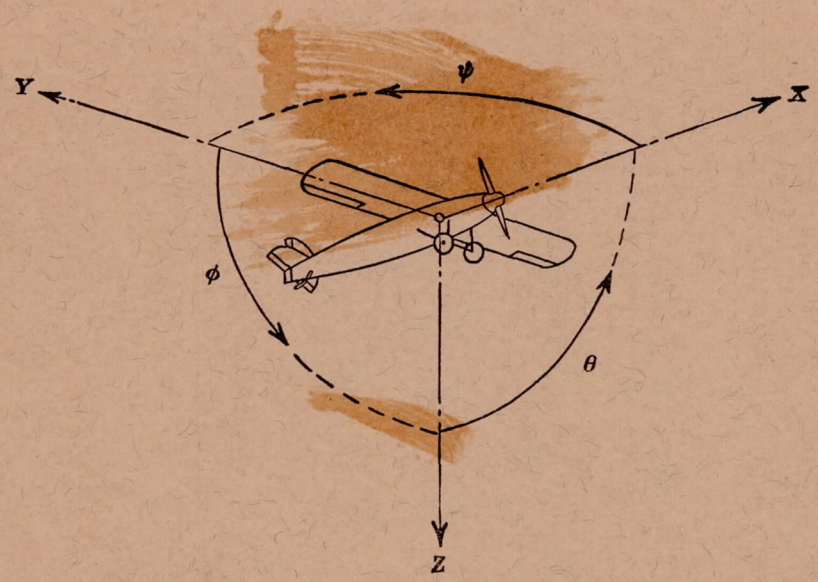

Positive directions of axes and angles (forces and moments) are shown by arrows

Axis		Force (parallel to axis) symbol	Moment about axis			Angle		Velocities	
Designation	Symbol		Designation	Symbol	Positive direction	Designation	Symbol	Linear (component along axis)	Angular
Longitudinal	X	X	Rolling	L	$Y \longrightarrow Z$	Roll	φ	u	p
Lateral	Y	Y	Pitching	M	$Z \longrightarrow X$	Pitch	θ	v	q
Normal	Z	Z	Yawing	N	$X \longrightarrow Y$	Yaw	ψ	w	r

Absolute coefficients of moment

$C_l = \frac{L}{qbS}$ (rolling) $\quad C_m = \frac{M}{qcS}$ (pitching) $\quad C_n = \frac{N}{qbS}$ (yawing)

Angle of set of control surface (relative to neutral position), δ. (Indicate surface by proper subscript.)

4. PROPELLER SYMBOLS

D Diameter

p Geometric pitch

p/D Pitch ratio

V' Inflow velocity

V_s Slipstream velocity

T Thrust, absolute coefficient $C_T = \frac{T}{\rho n^2 D^4}$

Q Torque, absolute coefficient $C_Q = \frac{Q}{\rho n^2 D^5}$

P Power, absolute coefficient $C_P = \frac{P}{\rho n^3 D^5}$

C_s Speed-power coefficient $= \sqrt[5]{\frac{\rho V^5}{P n^2}}$

η Efficiency

n Revolutions per second, rps

Φ Effective helix angle $= \tan^{-1}\left(\frac{V}{2\pi r n}\right)$

5. NUMERICAL RELATIONS

1 hp = 76.04 kg-m/s = 550 ft-lb/sec

1 metric horsepower = 0.9863 hp

1 mph = 0.4470 mps

1 mps = 2.2369 mph

1 lb = 0.4536 kg

1 kg = 2.2046 lb

1 mi = 1,609.35 m = 5,280 ft

1 m = 3.2808 ft